

Localized intrinsic bond orbitals decode correlated charge migration dynamics

Imam S. Wahyutama, Madhumita Rano, and Henrik R. Larsson

Department of Chemistry and Biochemistry, University of California, Merced, CA 95343, USA^{a)}

For decades, scientists have studied the intricate charge migration dynamics, where after ionization a localized charge distribution (“hole”) migrates across the molecule on a femtosecond timescale. This has the potential for controlling electrons in molecules, yet a comprehensive understanding of the many aspects of charge migration is still missing. In this work, we analyze charge migration using an extension of localized intrinsic bond orbitals (IBOs). These orbitals lead to a compact representation of the dynamics and map the complex, correlated many-electron charge migration to chemical concepts such as curly arrows and orbital-orbital interactions. By analyzing multiple challenging scenarios, we show how IBOs enable us to identify key mechanisms in charge migration. For example, we show that different mechanisms are responsible for converting a π -shaped hole to a σ -shaped hole and *vice versa*. We explain these in terms of hyperconjugation interactions and configurations that couple orbitals with different symmetries. We further demonstrate how IBOs can be used to find molecules with high charge migration efficiency. We carry out all simulations using an efficient set up of the time-dependent density matrix renormalization group (TDDMRG), correlating as many as 45 electrons in 50 orbitals. We believe that our results will be useful to design future experiments. The proposed IBO analysis is applicable to other types of real-time electron dynamics and spectroscopy.

I. INTRODUCTION

After a removal of an electron, how do the remaining electrons in a molecule respond, and how can this response be tuned and exploited? Answering this is central to the recently established field of attochemistry,^{1–4} and is useful to understand light-induced effects in DNA^{5,6} and photofragmentation,^{7–13} among many others.^{14–17} One particular response after an electron removal is charge migration, in which an often localized “charge cloud” or electron “hole” migrates through a molecule.^{8,10,18} Charge migration is initiated within attoseconds^{19–22} and leads to the initial hole migrating to the other end of small molecules such as aminoacids in just a few femtoseconds.^{23–27} So far, a plethora of simulations have investigated many properties and effects of charge migration, such as the controllability of the dynamics using ultrashort laser pulses,^{16,17} nuclei-induced decoherence effect,^{28–34} and molecular symmetry³⁵ or lack thereof,^{36–38} among others.^{25,39–46}

To systematically understand charge migration, we must identify universal patterns and rules that allow us to predict charge migration starting from different orbitals in different molecules.^{18,47–51} As the nonequilibrium, many-body, real-time electron dynamics of charge migration can be very complex and require the inclusion of electron-correlation effects,¹⁸ many tools have been used to analyze charge migration. Among others, these include various time-frequency analyses,^{18,47,48,52} density matrices (“hole density,” which we will define later) and their eigenstates (“natural charge orbitals”),⁴⁷ partial charges,^{53–55} electron fluxes,^{37,42,56–59} decompositions of the time-dependent wavefunction in terms of hole configurations,⁴⁷ and the time-dependent electron localization function.⁴¹ Despite these tools and both a large number

of simulations and experiments, many features of charge migration still remain elusive.^{49,60–66}

Next to the aforementioned ways to understand charge migration, quantum chemistry offers many more tools to gain insights by mapping the complicated many-body wavefunction to simple chemical concepts such as curly arrows⁶⁷ and atomic charges. Examples of such tools include energy decompositions,^{68–73} wave function tilings,^{74,75} entanglement patterns,^{76–78} and localized orbitals.^{79–87} Particularly, intrinsic bond orbitals (IBOs)⁸⁶ have been shown to be very useful, e.g., to verify empirical laws,^{86,88} to understand oxidation states,^{86,89,90} and to gain an understanding of chemical reactions in terms of curly arrow mechanisms,^{88,90–92} e.g., for gold catalysts,⁸⁹ electron transfer in proteins,⁹¹ and electron flow in chemical reactions.^{88,93} However, most of these use cases involve ground state electronic structures, with some exceptions covering excited eigenstates.^{94,95}

In this work, we extend the IBO formalism to describe real-time, correlated, nonequilibrium charge migration dynamics. We show that IBOs work well for describing charge migration even in complicated scenarios, and their localized and time-independent character makes IBOs easier to analyze than established quantities such as time-dependent natural charge orbitals. Surprisingly, we find that only a small amount of IBOs are required to semi-quantitatively describe correlated dynamics, even in charge migration that display typical features of what is described as “breakdown of the molecular orbital picture.”^{47,48}

Our analysis shows that known concepts to describe charge migration such as hole configurations are intuitively mappable to quantities derived from IBOs. Furthermore, we explain charge migration not only in terms of IBOs but also in terms of concepts that so far have rarely been used. Particularly, these include through-space orbital interactions in terms of hyperconjugations,⁹⁶ orbital interactions that are facilitated by local symmetries that do not extend over the whole molecule, and curly-arrow mechanisms using Lewis structures. Lastly,

^{a)}Electronic mail: p_cm26 [a t] larsson-research . de

we also show how IBOs help understand ionization spectra without resorting to real-time dynamics simulations.

We apply our developed concepts to various challenging scenarios. For example, we reveal that ionization from either the σ -bonding orbital or the π -bonding orbital of the carbonyl group in phenylacetaldehyde leads to charge migrating into the phenyl-ring σ bonds, despite the vastly different σ - and π -like initial charge distributions. Among others, we explain this in terms of through-bond and through-space orbital interactions such as hyperconjugation. These are easily identified by our IBO analysis. In stark contrast to phenylacetaldehyde, a similar type of ionization in the carbonyl group of furfural leads to a migration into the π orbitals of the furyl group, regardless of whether the initial orbitals are of σ or π character. We show that this can be explained through higher-order particle-hole configurations that are compactly described through bonding and antibonding IBOs. Finally, we reveal that two conformers of 3-fluoro-2-methylpropanal lead to different charge migration efficiencies, which is due to intricate interactions between three key IBOs. We believe that these insights help in the ongoing quest of finding molecules with long-lasting, coherent charge migration.^{34,52,97}

Simulating the nonequilibrium, correlated real-time charge migration electron dynamics is very challenging and significantly extends the usual application domain of electronic structure methods.⁹⁸ In this work, our simulations are based on a recently developed⁵⁵ efficient pipeline for the time-dependent quantum-chemistry density matrix renormalization group (TDDMRG).^{99–108} TDDMRG is inherently a multireference method and hence suitable for simulations like charge migration, where the time-dependent state can consist of a superposition of many highly excited configurations. Due to our efficient setup,^{55,106,107} our TDDMRG simulations significantly extend previous ones, and we are able to simulate fully correlated dynamics as large as phenylacetaldehyde with 45 electrons in 50 active orbitals. This, to our knowledge, sets a record for the largest TDDMRG simulation performed so far. Such a setup would be prohibitively expensive for many other multireference methods. We believe that both our TD-DMRG setup and our IBO analysis framework will be useful for other challenging simulations, such as ionization and excitation spectra in general,^{109–112} nonequilibrium dynamics of excited molecules,^{113–116} and of core-ionized molecules.¹¹⁷

The remainder of this paper is organized as follows. In Section II we overview theories and tools employed in the present work, including an extension to the IBO concept. We present the results of our simulations and analyze them in Section III. We conclude our findings and give our perspective of future use cases in Section IV.

II. THEORY

This Section is outlined as follows. In Section II A, we present an overview of the TDDMRG to simulate real-time electron dynamics. We can gain additional insights of such dynamics from ionization spectra, which we discuss in Section II B. In Section II C we review charge migration and com-

mon tools to analyze it. As a new tool to analyze charge migration, we give an overview of IBOs and their extensions in Section II D. Lastly, in Section II E we discuss global and local symmetries. Throughout, we use atomic units unless specified otherwise.

A. Time evolution using the density matrix renormalization group

We simulate electron dynamics by approximately solving the time-dependent Schrödinger equation using the TD-DMRG. In this method, the time-dependent state is expressed as a *matrix product state* (MPS),

$$|\Psi(t)\rangle = \sum_{\{\sigma\}} \left(\prod_{i=1}^K \mathbf{M}^{\sigma_i}(t) \right) |\sigma_1 \dots \sigma_K\rangle, \quad (1)$$

where K is the number of active spatial orbitals, $|\sigma_i\rangle$ denotes one of the four possible spin configurations in the i -th orbital, and $\mathbf{M}^{\sigma_i}(t)$ are matrices of size $D_{i-1} \times D_i$. The largest of the D_i 's is called *bond dimension*, D . The larger D , the better the approximation to the exact full configuration interaction state. By using the *ansatz* of Eq. (1) to find the extremum of the time-dependent variational principle, one obtains a set of coupled equations to solve for $\mathbf{M}^{\sigma_i}(t)$. A Lie-Trotter splitting uncouples these equations, which leads to an algorithm that, essentially, sequentially propagates one matrix $\mathbf{M}^{\sigma_i}(t)$ at a time. For more information, we refer to Refs. [101–103,108], Appendix A, and to our recently developed simulation pipeline.⁵⁵

B. Ionization spectra

While charge migration focuses on the time-dependent dynamics after ionization, analyzing it in terms of a time-independent view through ionization spectra provides an additional, helpful perspective, as it allows scientists to identify the relevant eigenstates that are contributing to charge migration.^{18,47} Through linear response theory, the spectrum can be obtained from the dynamics via the autocorrelation function $A(t)$,^{118,119}

$$A(t) = \langle \Psi(t=0) | \Psi(t) \rangle. \quad (2)$$

A Fourier transform of $A(t)$ leads to the photo-absorption spectrum P as a function of excitation energy E ,

$$P(E) = \lim_{\eta \rightarrow 0} \frac{1}{\pi \hbar} \Re \int_0^\infty \exp(iEt/\hbar) \exp(-i\eta t) A(t) dt. \quad (3)$$

To describe the experimental energy resolution, a finite value of η is used, which leads to a convolution of $P(E)$ with a Lorentzian,

$$L(E) = \frac{1}{\pi} \frac{\eta}{E^2 + \eta^2}. \quad (4)$$

As an alternative to the time-dependent approach, the spectrum can also be obtained by computing a Green's function $G(E)$ as

$$P(E) = -\Im\langle\Psi(t=0)|\hat{G}(E)|\Psi(t=0)\rangle, \quad (5)$$

with

$$\hat{G}(E) = \frac{1}{\pi} \lim_{\eta \rightarrow 0} \frac{1}{E + i\eta - \hat{H}}. \quad (6)$$

In practice, the time-dependent approach, Eq. (3) allows us to obtain the total spectrum with a finite resolution determined by the propagation time, whereas the time-independent Green's-function-based approach, Eq. (5), allows us to target particular peaks with a resolution determined numerically through a finite value of η (the smaller η , the higher the resolution but the more difficult it is to compute Eq. (5)). The spectrum is then described as a linear combination of Lorentzians.¹²⁰

The state $\hat{G}(E)|\Psi(t=0)\rangle$ provides further insights into the spectrum. Expanding it in terms of eigenstates $\{|u_i\rangle\}$ with energies $\{E_i\}$,

$$\hat{G}(E)|\Psi(t=0)\rangle = \frac{1}{\pi} \lim_{\eta \rightarrow 0} \sum_i \frac{\langle u_i | \Psi(t=0) \rangle}{E + i\eta - E_i} |u_i\rangle, \quad (7)$$

shows that $\hat{G}(E)|\Psi(t=0)\rangle$ has dominant contributions from eigenstates close to the target energy E , and, on resonance with $E \rightarrow E_i$, it turns into eigenstate $|u_i\rangle$ after normalization.

Expressing $|\Psi(t=0)\rangle$ as an MPS, Eq. (5) can be solved using DMRG-like procedures that consist of solving linear systems of equations sequentially for each of the matrices \mathbf{M}^{σ_i} in Eq. (1). For more details, we refer to Refs. [107,120–122].

C. Charge migration

Charge migration happens when, after ionization, a positively charged region or *electron hole* moves through the molecule on an ultrafast timescale of attoseconds to few femtoseconds. To model charge migration, we use the common^{8,9,12,47–49,123–126} sudden ionization approximation,^{127,128} and describe the initial state $|\Psi(0)\rangle$ by removing an electron from the ground state $|\Psi_{\text{GS}}\rangle$. In second quantization, this is described by

$$|\Psi(0)\rangle = \langle\Psi_{\text{GS}}|\hat{a}_i^\dagger\hat{a}_i|\Psi_{\text{GS}}\rangle^{-1/2} \hat{a}_i|\Psi_{\text{GS}}\rangle, \quad (8)$$

where \hat{a}_i is the annihilation operator of a localized orbital $|i\rangle$. Sudden ionization can be achieved, e.g., by using laser pulses with dominant frequencies that overlap with orbital energies of one particular functional group in the molecule. Next to sudden ionization, we assume that the nuclei are frozen during the electron propagation, which is a good assumption for the first few femtoseconds. While this setup is idealized, such simulations still illustrate charge migration, often lead to significant insights, and match experimental observables.^{18,26,47,48}

A central quantity of charge migration is the hole density $h(\mathbf{r}, t)$, which is defined as the difference of the spin-summed

ground-state one-particle density $\rho_{\text{GS}}(\mathbf{r})$ and the density $\rho(\mathbf{r}, t)$ of the ionized wavepacket at time t ,

$$h(\mathbf{r}, t) = \rho_{\text{GS}}(\mathbf{r}) - \rho(\mathbf{r}, t). \quad (9)$$

The contribution $q_i(t)$ of orbital $|i\rangle$ to $h(\mathbf{r}, t)$ is called hole occupancy, and computed as $q_i(t) = \langle i | \hat{h}(t) | i \rangle$, where $\hat{h}(t)$ is the corresponding operator of $h(\mathbf{r}, t)$. Following the definition of Eq. (9), compared to the neutral molecule, a point \mathbf{r} around the cation has an electron excess if $h(\mathbf{r}, t) < 0$, otherwise, it lacks electrons and contributes to an electron hole. Likewise, positive values of $q_i(t)$ correspond to a hole occupancy in orbital $|i\rangle$, whereas negative values correspond to an electron excess in that orbital, relative to the neutral molecule. Similar to natural orbitals, we can define time-dependent orbitals that diagonalize $\hat{h}(t)$. These are called natural charge orbitals and can help with the analysis.⁴⁷ However, their time-dependent and, in many cases, complex-valued character makes them more difficult to use than time-independent, real-valued orbitals.

Another useful way to analyze charge migration is to expand the time-dependent cationic state $|\Psi(t)\rangle$ in terms of configuration-interaction-based expansion,⁴⁷

$$|\Psi(t)\rangle = \sum_j c_j(t) \hat{a}_j |\Phi_{\text{GS}}\rangle + \sum_{r,k<l} c_{rkl}(t) \hat{a}_r^\dagger \hat{a}_k \hat{a}_l |\Phi_{\text{GS}}\rangle + \dots \quad (10)$$

where $|\Phi_{\text{GS}}\rangle$ is an approximation to the neutral ground state molecule. In many cases, $|\Phi_{\text{GS}}\rangle$ is a Hartree-Fock-based configurations but in our case, it will be the DMRG-approximated ground state, $|\Psi_{\text{GS}}\rangle$. The configurations or states $\hat{a}_j |\Phi_{\text{GS}}\rangle$ are called one-hole (1h) configurations and $\hat{a}_r^\dagger \hat{a}_k \hat{a}_l |\Phi_{\text{GS}}\rangle$ are called two-hole one-particle (2h1p) configurations. Since 2h1p configurations are formed through a removal of two electrons from $|\Phi_{\text{GS}}\rangle$ followed by an *addition* of another electron in a different orbital, the occurrence of 2h1p (and higher-order, 3h2p etc.) configurations can be identified by orbitals with negative hole occupancies. In many cases, these orbitals are of antibonding character, and their occupancy weakens the corresponding bond. Further, 2h1p configurations are important to understand correlation effects and the occurrence of orbitals with different symmetries, as the orbitals involved in 2h1p configurations can have different irreducible representations (irreps). We will discuss this below in Section II E and Section III B.

D. Intrinsic bond orbitals and their extensions

Appropriately localized orbitals that resemble those from qualitative molecular orbital theory every chemistry student learns in their first lectures provide a direct mapping from *ab initio* electronic structure to chemical concepts such as bond analyses, localized charges and oxidation states. Consequently, a plethora of different localization procedures exist.^{81,85,87,129–134} Here, we use IBOs, which are convenient to create and which provide orbital shapes that match chemical intuition.⁸⁶ The original IBO procedure is for bonding orbitals. Below, we discuss an extension to antibonding orbitals.

The main ingredient in the construction of IBOs is the *intrinsic atomic orbitals* (IAOs). IAOs are orbitals centered around atoms that are not only localized but also encode the polarization environment of the molecule. IAOs are computed by projecting n_{\min} free-atom minimal basis set orbitals onto Hartree-Fock (HF) occupied and unoccupied molecular orbitals (MOs) that are computed by a larger basis set. The information on the polarization environment is inscribed into IAOs through this involvement of HF orbitals. IBOs are then constructed by localizing the n_{occ} occupied HF MOs using a variation of Pipek-Mezey orbital localization,⁸¹ which minimizes the number of atoms an orbital is centered on using IAO-based atomic charges. Thus, the IBOs span exactly the same space as the occupied MOs and generate the same single-determinantal wavefunction. In many cases, the shape of the IBOs corresponds remarkably well to textbook-like MOs, which makes IBOs very useful for understanding complex bonding scenarios.

For excited states and non-equilibrium dynamics such as those occurring in charge migration, excited configurations with occupied antibonding orbitals play a crucial role. However, by construction, IBOs are all bonding. To generate antibonding orbitals, we here extend the IBO procedure in a straightforward way using split localization. As we have n_{occ} IBOs, we generate $n_{\min} - n_{\text{occ}}$ localized, antibonding orbitals that we dub here *complementary IBOs* (cIBOs). These cIBOs are related to, e.g., the valence-virtual orbitals from Refs. [87,133], and have previously been generated by similar procedures.^{94,135,136} We generate cIBOs by first projecting the n_{\min} IAOs $\{|a\rangle\}$ into the space orthogonal to the IBOs $\{|i\rangle\}$, $|v\rangle = \left(\hat{1} - \sum_{i=1}^{n_{\text{occ}}} |i\rangle\langle i|\right) |a\rangle$. We then remove linearly dependent vectors from the set $\{|v\rangle\}$ using singular value decomposition, which gives a set of $n_{\min} - n_{\text{occ}}$ orthogonal orbitals.¹³⁷ We localize these orbitals to obtain the cIBOs in the same way the IBOs are constructed by using Pipek-Mezey localization with IAO-based atomic charges. By construction, the cIBOs form a set of localized orbitals that are orthogonal to the IBOs, and the union of IBOs and cIBOs exactly spans the same space as that of the IAOs. Hence, in the following, when no context is needed, we will collectively refer to IBOs or cIBOs as just IBOs.

IBOs and cIBOs together form a valence-internal space⁸⁷ and in most cases will suffice for a comprehensive qualitative analysis of our electron dynamics. The remaining orbitals correspond to what is called hard virtual space⁸⁴ or valence-external space.⁸⁷ Here, we dub these remaining orbitals oIBOs, where ‘‘o’’ refers to the fact that these orbitals are orthogonal to the IBO space. While this is not important for our results below, we localize the oIBOs in the same way we localize the other IBOs.

E. Global and local symmetries

To characterize hole motion in our electron-dynamics analysis, we distinguish global and local symmetries. Global symmetry refers to the irrep of the molecular point group. Local

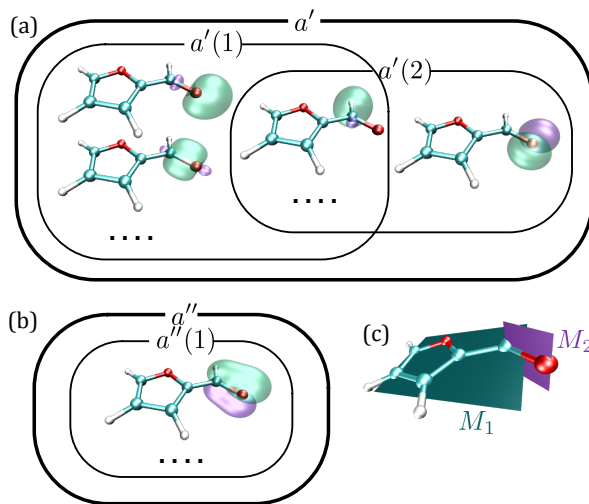


Figure 1: Comparison of global and local symmetries. (a, b)

Venn-diagram illustrations of the relationship between the global and local symmetries for the IBOs localized around the C=O bond in furfural. (c) The two mirror planes that define the global (M_1) and local (M_2) symmetries illustrated in the

Venn diagrams. The local symmetries are labeled as $a'(x)$ and $a''(x)$, respectively, where x arbitrarily enumerates them.

symmetry is an additional classification within a spatially restricted region spanning only a subset of atoms. The role of global symmetry in charge-migration dynamics has been explored previously,^{35–38} and mainly leads to the appearance of orbitals whose symmetry differs from that of the total wavefunction, which is often due to the 2h1p configurations defined in Eq. (10).

As shown below, restricting symmetry to local molecular regions — rather than the molecule as a whole — provides a useful framework for interpreting key features of charge migration. Such local symmetry is meaningful only for localized orbitals. This is not a restriction, as the wavefunction is invariant under a unitary transformation that localizes the orbitals. Unlike other uses of local symmetry in different contexts,^{138,139} we apply local symmetry here as an approximate classification and neglect small IBO distortions that violate the chosen local symmetry.

Fig. 1 highlights the interplay of global and local symmetries in selected IBOs of the C_s -symmetric furfural. The orbitals in panel (a) transform as a' because they are even under reflection in the molecular plane M_1 in panel (c), whereas the orbital in panel (b) transforms as a'' due to its odd M_1 parity. Focusing on the formyl group, the a' orbitals can be further classified by their parity with respect to a second reflection plane M_2 defined in panel (c), which contains the C=O bond and is perpendicular to M_1 . This leads to a local symmetry with irreps $a'(1)$ and $a'(2)$ that denote even and odd M_2 parity, respectively. Orbitals from different global irreps necessarily fall into different local symmetries, but some orbitals lack a particular local symmetry. These can be decomposed into orbitals with different symmetries, as indicated by the overlap of the Venn diagrams for $a'(1)$ and $a'(2)$. Next to the local sym-

metries shown in Fig. 1, other local symmetries are possible for furfural.

III. RESULTS AND DISCUSSIONS

In the following, we present our investigation of charge migration dynamics using IBO hole occupancies as the main tool of analysis. We start by validating the IBO-based analysis in simple linear molecules in Section III A. We then apply it to study changes of hole symmetries in the charge migration of phenylacetaldehyde and furfural in Section III B, followed by revealing different charge migration efficiencies in conformers in Section III C. Details on the computational set up are given in Appendix A and in the Supporting Information.

A. Validation of the IBO-based analysis in linear molecules

Linear molecules are the most suitable ones for studying and observing charge migration due to the presence of only one possible migration route. One of the first experimental observations of charge migration was made in a linear molecule.²⁶ A number of theoretical works have also studied charge migration dynamics in linear molecules.^{44,45,47–49,52,60,140,141} The properties of the migration dynamics in terms of molecular length, functional group, and initial hole, among others, are investigated in these works. In Section III A 1 and Section III A 2, we analyze ultrafast electron dynamics in chloroacetylene and chlorobutadiyne, respectively, to demonstrate that our IBO-based analyses work for the simple scenario of charge migration in a linear molecule, before we continue with more challenging scenarios.

1. Chloroacetylene

One of the first experiments that revealed charge migration was done with iodoacetylene.²⁶ Therein, scientists observed that an initial p hole, starting from iodine, migrates to the other end of the molecule and back to iodine in about 1.9 fs. The initial state for that dynamics is approximately a 50-50 superposition of the ground state $|u_0\rangle$ and first excited state $|u_1\rangle$ of the cation. In general, for such superpositions of the cationic state, $|\Psi(t)\rangle = c_0|u_0\rangle + c_1|u_1\rangle$, the hole density is given by

$$h(\mathbf{r}, t) = \rho_{GS}(\mathbf{r}) - c_0^2\rho_0(\mathbf{r}) - c_1^2\rho_1(\mathbf{r}) - 2c_0c_1\rho_{01}(\mathbf{r})\cos(\Delta Et/\hbar), \quad (11)$$

where ρ_0 and ρ_1 are the electron densities of $|u_0\rangle$ and $|u_1\rangle$, respectively, ρ_{01} is the transition density between these two eigenstates, and ΔE is their energy difference. Such a situation has been dubbed *hole mixing*.⁴⁷

Here, as a first test of our procedure, we model the iodoacetylene charge migration experiment using chloroacetylene, which, compared to iodoacetylene, has fewer electrons and weaker relativistic effects. This makes it easier to simulate. Our TDDMRG simulation uses a bond dimension of

$D = 1,000$ and an active space of CAS(15e,41o), which stands for 15 electrons in 41 orbitals. In this case, this corresponds to the full orbital space (full configuration interaction) when using the frozen core approximation (7 frozen orbitals) and the def2-SV(P) basis. We construct the initial state by removing an electron from the neutral in an orbital that is a superposition of the HF HOMO and HOMO-1. As in the iodoacetylene experiment, this state exhibits a p hole in chlorine.

The snapshots of the evolving hole density in chloroacetylene are shown in Fig. 2(a). Given that only the cationic ground state and the first excited state should dominate the dynamics, we expect that also only two IBOs will be dominant.¹⁴² Indeed, only two IBOs contribute to the hole density. To gauge how well the two dominant IBOs reproduce the dynamics, we recompute the hole density using just these two dominant IBOs, ignoring all other orbitals, and show it in Fig. 2(b). The main hole lobes (positive, green surfaces) in Fig. 2(a) are faithfully reproduced by the two IBOs. The missing features in the IBO-projected hole density are mostly electron lobes (negative, purple surfaces), which are mainly located near the molecular axis. These differences are due to additional correlation effects not accounted for when using the two dominant IBOs only. Importantly, by using the *full* IBO, cIBO, and oIBO spaces, the dynamics can be exactly reproduced.

The shapes and the time-dependent hole occupancies of the two dominant IBOs are shown in Fig. 2(c). They are close to the initial p hole state at the Cl atom (IBO-1) and a π hole state at the C=C bond (IBO-2). In agreement with Eq. (11), the hole occupancies exhibit a clear periodic oscillation with a period of ~ 1.29 fs. To further confirm this, Fig. 2(d) compares the absolute value of the autocorrelation function, $|A(t)|$ with a reproduction from the 2-state model in Eq. (11). As the hole density reproduced with two IBOs only, the two-state autocorrelation function closely resembles the TDDMRG reference.

As discussed in Section II C, a common way to analyze charge migration is to use time-dependent natural charge orbitals, obtained by diagonalizing the hole density at different time steps. The densities of the three most dominant natural charge orbitals at different times are shown in Fig. 2(e)-(i). For all times shown, the most dominant natural charge orbital reproduces the hole density almost as good as the two IBOs. Note that some small details are better captured by the two IBOs than by the dominant natural charge orbital, e.g., a small contribution to the hole density at the Cl atom at 0.648 fs. Like the excluded IBOs, the additional natural charge orbitals lead to a full reproduction of the hole density. However, unlike IBOs, the natural charge orbitals do not directly reveal the two-state characteristic of the dynamics. The time dependence of the natural charge orbitals and, in most scenarios, their complex-valued nature further complicate an analysis based on them.

Previously, IBOs have been used to draw curly-arrow mechanisms of chemical reactions by analyzing IBOs along reaction paths.^{88,90–92} For the simple charge migration scenario of chloroacetylene, we follow a similar procedure but analyze the IBOs not along a reaction path but along the real simulation time for a fixed nuclear structure. We first map each of the

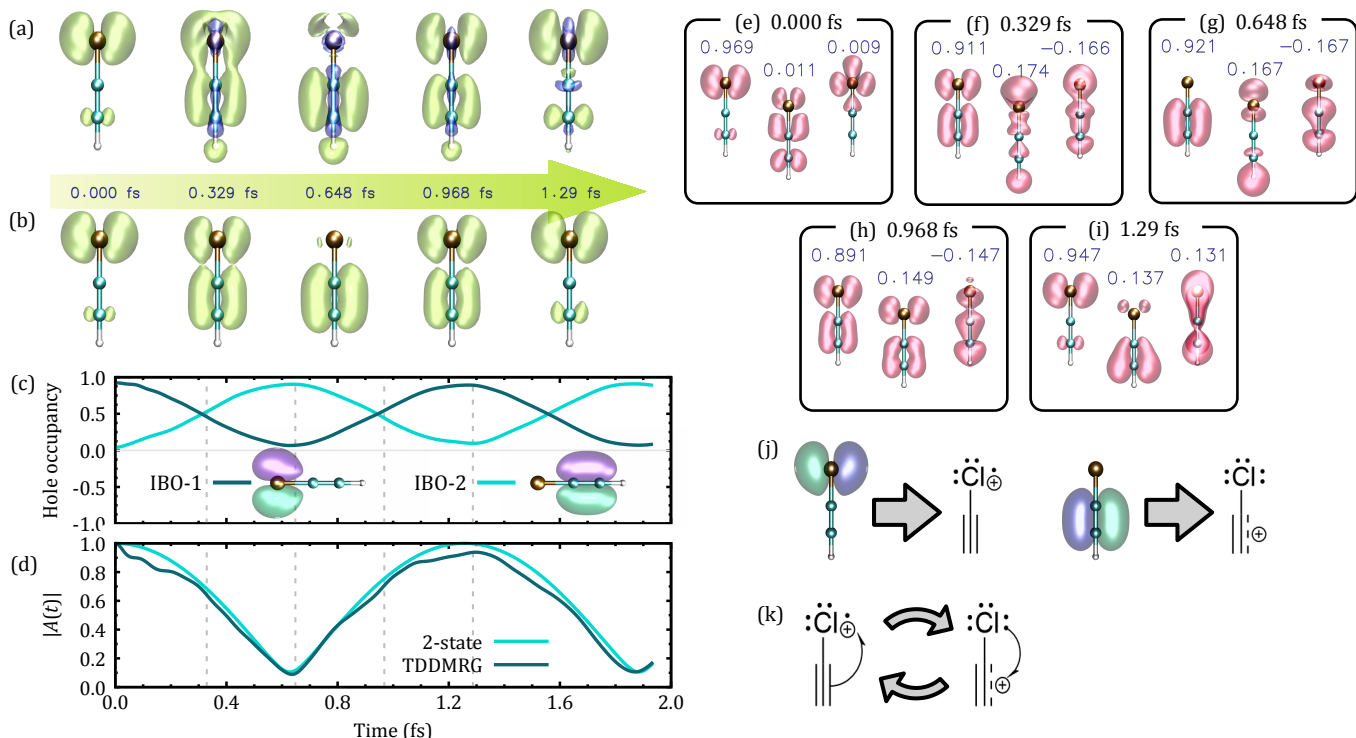


Figure 2: Charge migration analysis of chloroacetylene. (a) Hole density snapshots. Regions with positive (negative) density are shown as green (purple) lobes. (b) Hole density snapshots obtained by projecting the density from (a) to the space of the two dominant IBOs. (c) Hole occupancies of the two IBOs that dominate the hole dynamics. The IBOs are shown on the graph. The times at which the snapshots in (a) are taken are indicated with dashed vertical lines. (d) Absolute value of the autocorrelation function (dark green curve) in comparison to a two-state model (cyan curve). (e)-(i) Orbital densities of the three most dominant (largest absolute eigenvalues) natural charge orbitals at the times of the snapshots in (a). (j) Mapping of IBOs to cationic Lewis structures. (k) Curly-arrow representation of the periodic hole oscillations.

two IBOs to Lewis structures of the cation, see Fig. 2(j). Following the hole occupancy analysis in Fig. 2(c), we then identify the main Lewis structures at times when only one of them dominates and connect them through curly arrows as shown in Fig. 2(k). As the single-headed curly arrows (harpoons) correspond to the “motion” of a single electron, their direction is opposite to the motion of the electron hole.¹⁴³ For this simple case, the Lewis-structure mechanism fully agrees with Eq. (11).

2. Chlorobutadiyne

Studying charge migration in linear molecules longer than chloroacetylene helps elucidate how the back-and-forth periodic motion depends on molecular length and how this, in turn, impacts the IBO decomposition. Accordingly, we simulate charge migration in chlorobutadiyne using TDDMRG with a CAS(23e, 45o). Similar to chloroacetylene, we start with a p hole at the Cl atom, which we created from the corresponding IBO.

Fig. 3(a) depicts snapshots of the hole density throughout the 4-fs simulation. We find that a sizeable portion of the hole migrates to the terminal C=C bond and back to Cl within

1.91 fs (see the red arrow). A similar round-trip time of 2.38 fs was observed from RT-TDDFT simulations in Ref. [49]. Compared to our value, the difference of 0.47 fs is due to different initial states, geometry, and the propagation method employed in Ref. [49].

There are three dominant IBOs, shown in Fig. 3(d), that reproduce the qualitative features of the dynamics. As in chloroacetylene, two IBOs correspond to the p orbital of the Cl atom and the π -orbital of the C=C bond next to the Cl atom, respectively. Since chlorobutadiyne contains an additional conjugated C=C pair, a second π orbital localized on that pair is the third dominant IBO. The reproduction of the hole density using only these three IBOs is shown in Fig. 3(b). Additional features of the hole density stemming from electron correlations can be reproduced by including more IBOs.

Next to assessing the truncated IBO expansion through the hole density, another useful check is to inspect the sum of all hole occupancies, which must equal 1 in the complete orbital space. Fig. 3(c) compares this quantity for different orbital subsets. Using only the three dominant IBOs leads to a summed occupancy slightly larger than 1 with a maximum value of 1.08 (dark green). Surprisingly, adding the remaining IBOs (while excluding antibonding cIBOs) degrades the summed occupancy and leads to a maximum value of 1.24

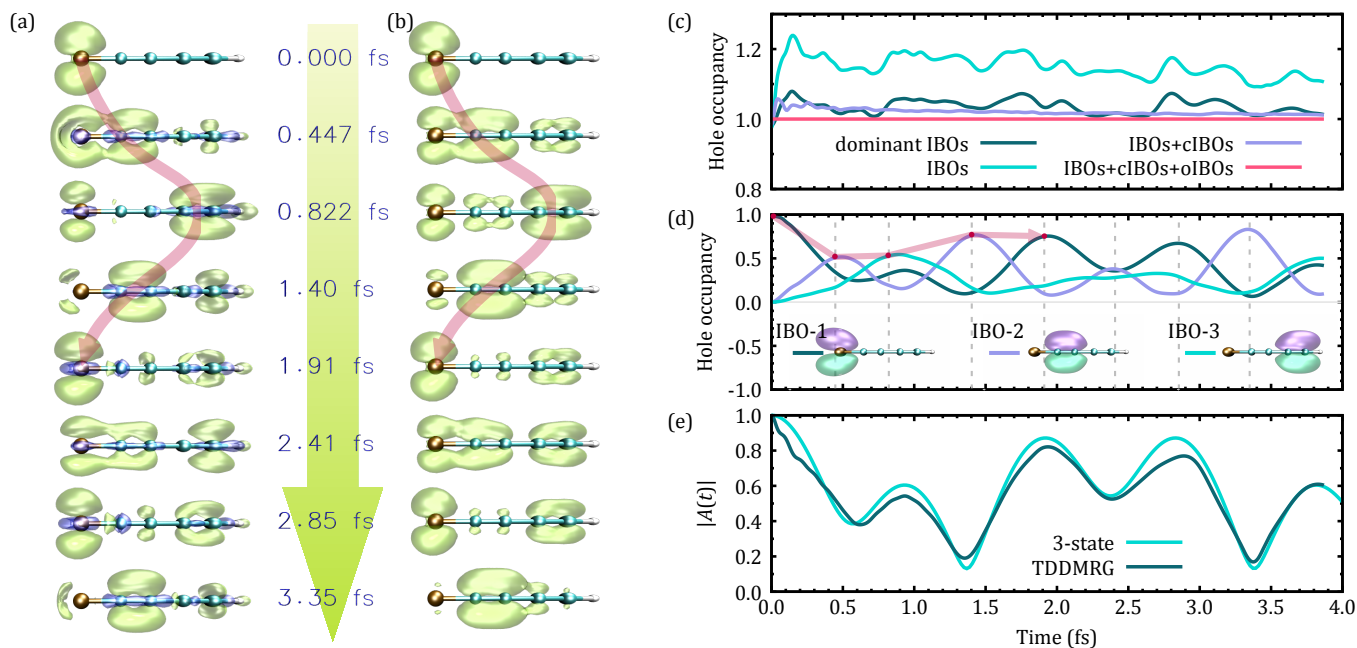


Figure 3: Charge migration analysis of chlorobutadiyne. (a) Hole density snapshots. The color code is the same as that in Fig. 2(a). The arrows signify the quasiparticle-like characteristics of the dynamics within the first 2 fs. (b) Snapshots of the hole density in (a) projected into the space of the three most dominant IBOs. (c) Sum of hole occupancies within the subspaces of the three dominant IBOs, IBOs, IBOs \oplus cIBOs, and IBOs \oplus cIBOs \oplus oIBOs. (d) Shapes and hole occupancies of the three dominant IBOs. (e) Absolute value of autocorrelation function (dark green) in comparison to a 3-state model (cyan).

(cyan). The result improves only once the antibonding cIBOs are included (purple). Adding the oIBOs completes the space and restores the exact value of 1 (red).

Why can IBOs alone worsen the summed hole occupancy? The orbital hole occupancy can be positive or negative; negative values indicate electron excess relative to the neutral ground state and typically are caused by contributions from antibonding orbitals in the cationic nonequilibrium state (see Section II C). Because cIBOs are antibonding by construction and thus typically lead to negative occupancies, they can be as important for reproducing the dynamics as the bonding IBOs. Dominant antibonding orbitals with negative occupancies are discussed in more detail in Section III B.

The time-dependent hole occupancies of the three dominant IBOs are shown in Fig. 3(d). By tracking the peaks of these curves and keeping in mind where the IBOs are localized at, we can qualitatively follow how the hole migrates through the molecule within the first 2 fs (compare the red arrows in Fig. 3(a) and (d)). At later times, the hole density becomes more delocalized, which is also reproduced by multiple IBO contributions at a given time. For example, at 2.41 fs, all three IBOs have almost similar contributions.

Following the analysis of chloroacetylene, we can model the dynamics in chlorobutadiyne using a three-state model, which reproduces the autocorrelation function well, as shown in Fig. 3(e). As for chloroacetylene, this good agreement and the three dominant IBOs reveal that the dynamics is mainly due to a superposition of the ground and the two lowest excited states.

B. Effects of the initial hole symmetry

The dynamics of the linear molecules in Section III A are relatively simple, for instance, the dominant IBOs all share the same global symmetry as the initial hole. In the remainder, we will analyze charge migration in more complicated scenarios—phenylacetaldehyde in Section III B 1 and furfural in Section III B 2, which reveal both local and global symmetry effects.

1. Phenylacetaldehyde

Our first more complex charge migration scenario is that of a C_s -symmetric conformer of phenylacetaldehyde that is eclipsed between the carbonyl group and the phenyl group; see Fig. 4(a). This raises the question of how an initial hole at the carbonyl group migrates into the phenyl ring and how this depends on the hole's symmetry with respect to the phenyl-ring plane. To answer this, we perform three TDDMRG simulations with different initial holes, each localized at the carbonyl group: 1) a σ hole, 2) a π hole, and 3) a hole in the O atom's p lone-pair orbital. We refer to the resulting dynamics as σ , π , and p dynamics, respectively. See the leftmost panels in Figs. 4(a)-(c) for the shapes of the initial holes.

Snapshots of the hole densities during these three dynamics are shown in Fig. 4(a)-(c). The hole occupancies of dominant IBOs localized at the 2-oxoethyl group are shown in Fig. 4(d),

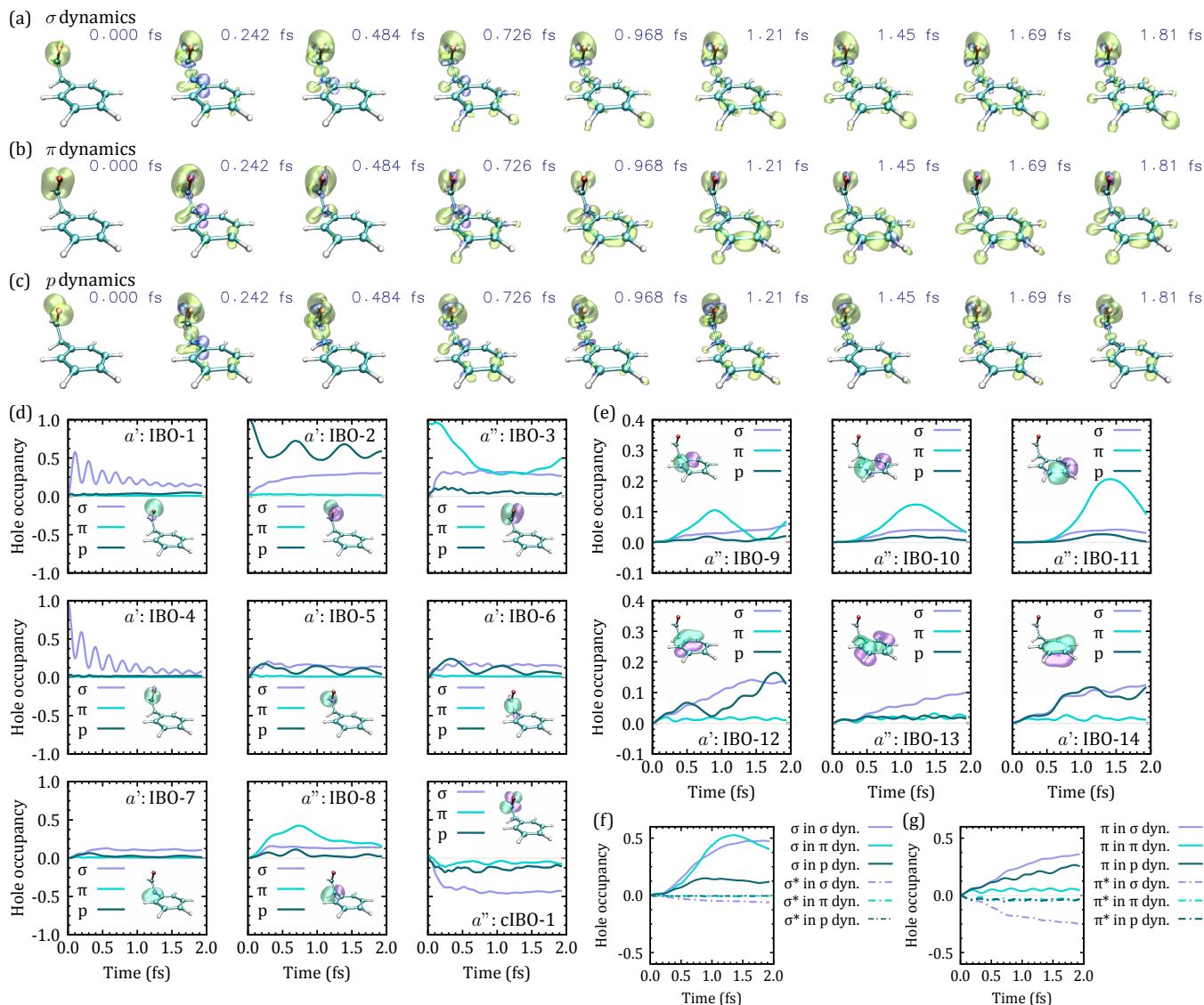


Figure 4: Charge migration analysis of phenylacetaldehyde. (a)-(c) Hole density snapshots for the σ , π , and p dynamics, respectively. The color code is the same as that in Fig. 2(a). (d) Hole occupancies of IBOs localized in the 2-oxoethyl group during the three dynamics. The IBO associated with each hole occupancy and its irrep label are shown in each panel. (e) Hole occupancies of selected σ and π IBOs localized at the phenyl group. Note that the ordinate range differs from that in (d). (f, g) summed hole occupancies of IBOs within the phenyl ring having σ and π local symmetries, respectively. This includes IBOs localized at the H atoms and those shown in (e).

while the occupancies of selected IBOs localized at the phenyl ring are shown in Fig. 4(e) (the other phenyl IBO occupancies are depicted in Supplementary Fig. S1). Furthermore, we display summed hole occupancies of all phenyl IBOs in Fig. 4(e, f) for σ and π IBOs, respectively. Note that, here, σ and π refers to the local symmetry with respect to the phenyl plane.

The three dynamics have various features that can be explained by different physical mechanisms. In the following, we analyze and discuss three particular mechanisms and the resulting dynamics: (a) hyperconjugation-based through-space orbital interactions that are responsible for different charge migration efficiencies and that lead to a change of hole shape

when migrating from the carbonyl group into the phenyl ring; (b) excited $2h1p$ configurations that lead to the appearance of orbitals with different global symmetries; and (c) the “break-down of the molecular orbital picture” that leads to quasi-exponential decays of IBO hole occupancies for the σ and p dynamics. We summarize these effects in Table I.

a. Hyperconjugation modulates charge migration efficiency and converts the local hole symmetry A striking difference between the three dynamics is the amount of charge migration into the phenyl ring. For the time range studied, the p (π) dynamics exhibits the smallest (largest) migration, and the maximum total hole occupancy in the ring is 0.34 (0.53).

Table I: Changes of the hole symmetry in phenylacetaldehyde. For each dynamics, the hole conversion is shown next to the relevant IBOs at the 2-oxoethyl group and at the entry of the phenyl group (c.f. Fig. 4), and a qualitative explanation. For the change of local symmetry, the initial hole symmetry corresponds to that of the orbital at the CO group.

| Local symmetry | | | |
|--------------------------------|------------------------------|--------------------|---|
| Dynamics/initial hole symmetry | Hole symmetry in the Ph ring | Relevant IBOs | Hyperconjugations around Ph entry |
| σ | $\sigma + \pi$ | 4-8, 12 | $\sigma - \sigma$ and $\sigma - \pi$ |
| π | σ | 3, 8, 9 | $\sigma - \sigma$ |
| p | π | 2, 5-9, 12 | $\sigma - \pi$ |
| Global symmetry | | | |
| Dynamics/initial hole irrep | Final hole irreps | Most relevant IBOs | Explanation |
| $\sigma (a')$ | $\sigma (a') + \pi (a'')$ | 3, 4, cIBO-1 | Coupling through 2h1p configurations; "orbital breakdown" |

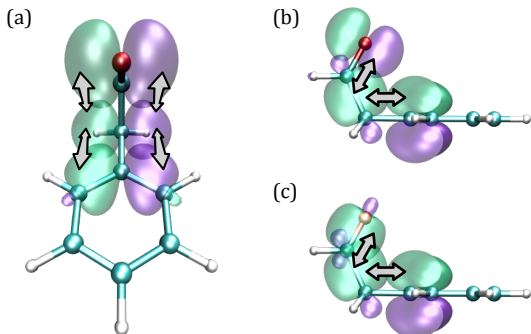


Figure 5: Main IBOs taking part in the hyperconjugation interactions in phenylacetaldehyde. (a) π , (b) p , and (c) σ dynamics. The interactions lead to ring σ holes in the first and ring π holes in the last two dynamics, respectively. The arrows indicate the interactions.

Compared to the π dynamics, the σ dynamics features a similar amount of migration into the ring, whose origin we will discuss later in the context of 2h1p configurations and global symmetries.

In conjunction with different charge migration efficiencies observed above, for all three dynamics, the initial hole changes its local symmetry when migrating from the carbonyl group into the phenyl ring as follows: 1) $\sigma \rightarrow \sigma + \pi$, 2) $\pi \rightarrow \sigma$, and 3) $p \rightarrow \pi$. This is most noticeable from the phenyl IBO hole occupancies in Fig. 4(e), and from the summed phenyl IBO occupancies in panels (f) and (g). Changes in local hole symmetry are also evident in the time-dependent natural charge orbitals (Supplementary Fig. S3), but the time-independent, localized IBOs dramatically speed up the analysis and thus are shown here.

This change of local symmetry is most obvious for the π dynamics, as shown by the hole density at $t = 0.968$ fs in Fig. 4(b) and by the selected phenyl σ IBO occupancies in panel (e). What leads to these ring σ holes? Initially, the C=O π hole (IBO-3) migrates into the two mirror-symmetric C-H σ bonds of 2-oxoethyl; compare the initial hole density with that at $t = 0.242$ fs in Fig. 4(b) and the occupancies of

IBO-8 in panel (d). Note that, aside from IBOs 3 and 8, no other 2-oxoethyl IBOs have large occupancies. After arriving at the C-H IBO-8, the hole migrates through the nearby phenyl C-C σ IBO-9 in the ring, compare the snapshots at $t = 0.484$ fs and $t = 0.726$ fs in panel (b), and the σ -ring IBO occupancies in panel (e).¹⁴⁴ Comparing the occupancies of IBOs 9 and 10 shows that migration from one end of the ring to the other requires only 0.5 fs.

Qualitatively, we explain both the different charge migration efficiencies and the change of local symmetries in terms of hyperconjugations/through-space orbital interactions⁹⁶ that occur as the hole migrates down the 2-oxoethyl group and arrives at the entry point into the ring.¹⁴⁵ Fig. 5(a) illustrates this mechanism. These interactions first occur between the initial C=O π IBO-3 and the C-H σ IBO-8. Once the hole reaches the latter IBO, additional interactions occur with the nearby phenyl C-C σ IBO-9, leading to the migration into the ring.

In contrast to the π dynamics, the p dynamics leads to π character in the ring. Note that there is no π -type conjugation visible in phenyl in Fig. 4(c), instead, we see p -orbital-shaped lobes on the C atoms. However, plots at a different isosurface value reveal conjugation. We confirm this from the π IBO occupancies in panel (e) and from the summed IBO hole occupancies in panels (f) and (g), where, for the shown time range, the summed π ring IBO occupancy of the p -dynamics reaches a maximum value of 0.22, whereas that of the σ ring IBOs is only 0.14.

The change of local symmetry in the p dynamics is due to the 2-oxoethyl C-C σ IBO 6, which interacts through hyperconjugation with the phenyl π IBO-12, as shown in Fig. 5(b). IBO 6 is not active in the π dynamics, as its symmetry is different to that of the initial hole. A similar analysis holds for IBO 5. The limited interactions between the initial p hole (IBO-2) and the C-H σ -bonding IBOs 7 and 8 leads to a reduced migration into the ring through these IBOs and consequently almost no σ holes in the ring for the p dynamics.

The σ dynamics lead to hole densities in the ring of both σ and π character. Because the initial IBO-4 is mirror-symmetric, like the p -type IBO-2, the same orbitals active in the p dynamics give rise to the π -ring hole occupancies; see Fig. 4(e) for the occupancies and Fig. 5(c) for the mechanism.

Through another mechanism that we will explain in the next paragraph, in the σ dynamics, the π IBO-3 becomes active and hence also leads to active σ ring IBOs.

b. 2h1p interactions lead to a change of global hole symmetry In the preceding paragraph, we have analyzed how the hole shape and thereby its local symmetry changes when migrating from the carbonyl group into the phenyl ring. Now, we shift our analysis to a change of the global symmetry, i.e., the occurrence of dominant hole orbitals with irreps different from that of the initial hole. This can occur through an excitation mechanism that contain orbitals with different irreps.⁴⁷ Note that this does not affect the symmetry of the total wavefunction, which is conserved.

This global symmetry effect is very pronounced in the σ dynamics, where within the first 0.8 fs the occupancy of the initial hole in the σ -type C=O IBO-4 (a') rapidly decreases while other IBOs become dominant, particularly the positive occupancy of the π -type C=O IBO-3 (a'') and the negative occupancy of the π^* cIBO-1 (a''), c.f. Fig. 4(d). These orbitals of different global symmetries are coupled through excited configurations as shown in Eq. (10): the initial state corresponds to a one-hole (1h) configuration, $\hat{a}_{\text{IBO-4}}^\dagger |\Psi_{\text{GS}}\rangle$, and it couples with 2h1p configurations of type $\hat{a}_{\text{cIBO-1}}^\dagger \hat{a}_{\text{IBO-3}} \hat{a}_{\text{IBO-X}} |\Psi_{\text{GS}}\rangle$, where X is one of the orbitals of a' symmetry whose hole occupancy is increasing, e.g., $X = 5$, while that of cIBO-1 is decreasing. The 2h1p configurations with electrons in the π^* C=O bond weaken this bond and hence facilitate the charge migration into other regions of the molecule. Through this mechanism, the π -bonding C=O IBO-3 becomes active during the σ dynamics and enables a similar mechanism and charge migration efficiency as that of the π dynamics.

When starting from a 1h state, couplings to 2h1p states and higher-order states (3h2p etc.) are easily recognizable by the appearance of negative occupancies in the antibonding cIBOs. For example, common for all three dynamics is a negative p -type lobe in the hole density of the phenyl ring at 0.242 fs in Fig. 4(a). This leads to very similar π and π^* ring IBO occupancies at the onset of the dynamics, c.f., Fig. 4(e) and Supplementary Fig. S1, where negative occupancies of π^* IBOs are shown. As another, related example, at later times, once the ring becomes populated, the σ dynamics exhibit large negative occupancies in the antibonding π orbitals of the phenyl ring; see Fig. 4(g). However, the occupancies of the π and π^* IBOs almost cancel each other and the maximum value of the combined π and π^* occupancy is 0.11, which explains why only a few π -like features are visible in the hole density in Fig. 4(a). The large negative occupancies in the σ dynamics that are due to many 2h1p configurations indicates that there are many more states in the σ dynamics that are excited than in the other two dynamics. We will analyze this in more detail in the next paragraph.

c. The “breakdown of the molecular orbital picture” leads to damped oscillations Both the σ and p dynamics lead to quasiexponentially decaying oscillations of IBO occupancies; compare the the hole occupancies in Fig. 4(d) of IBOs 1, 4, 5, and 6 for the σ dynamics and that of IBOs 2, 5, and 6 for the p dynamics, respectively. This quasiexponential decay has previously been analyzed by Breidbach and Cederbaum,^{47,48} and

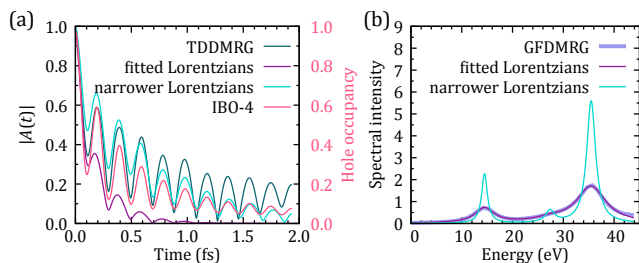


Figure 6: Autocorrelation function and ionization spectrum of the σ dynamics of phenylacetaldehyde. (a) TDDMRG autocorrelation function (dark green), Fourier transforms of the fitted Lorentzians from the ionization spectrum in panel (b) (purple), the same but with an artificially decreased width to match the autocorrelation (cyan), and IBO-4 hole occupancy from Fig. 4(d) (red). (b) DMRG ionization spectrum of the σ dynamics (light purple), fit to three Lorentzians (purple), and the same fit but with decreased Lorentzian widths by a factor of 0.3 (cyan).

was identified as a signature of a highly correlated initial state produced by an ionization of a core orbital or, as in our case, an inner valence orbital. A signature of such a scenario are contributions to the initial state from a quasicontinuum of states in the ionization spectrum. Consequently, this scenario is dubbed “breakdown of the molecular orbital (MO) picture.”¹²⁸

In the following, we will analyze this behavior for the σ dynamics, where it is most dominant. Indeed, the initial state in the σ dynamics corresponds to inner valence ionization with an ionization potential of 34 eV, which is a typical energy for an orbital breakdown. The exponentially damped oscillation is not only visible in the hole occupancies, but also in the autocorrelation function in Fig. 6(a), dark green curve. Remarkably, the autocorrelation closely corresponds to the hole occupancy of IBO-4 (red) for all shown times. We used this IBO to create the initial state.

The ionization spectrum provides further insights (see Section II B), and it is shown in Fig. 6(b) as light purple curve. While these spectra are difficult to converge, with the used spectral broadening of $\eta = 0.08$, we clearly see two peaks at 14.5 eV and 35.5 eV, and a shoulder near 27.4 eV. The shoulder is due to another peak, which we confirmed through unconverged computations with smaller broadening (not shown). Note that the used broadening does not allow for a resolution at the eigenstate level, so we assume that multiple eigenstates contribute to the peaks. These observations are in full agreement with the breakdown of the MO picture.⁴⁸

Fitting the spectral intensity $P(E)$ with three Lorentzians $L(E)$ defined in Eq. (4), $P(E) = \sum_{i=1}^3 A_i L(E - E_i)$, fully reproduces the computed spectrum (dark purple curve in Fig. 6(b)); see Supplementary Table S9 for the fit parameters. A Fourier transform of $P(E)$ reproduces the main oscillations and quasiexponential decay of the autocorrelation function (dark purple curve in Fig. 6(a)), but, because of the large broadening used in our simulation, overestimates the decay. However, we can artificially narrow the Lorentzians (cyan curve in panel (b)), and the Fourier transform in panel (a) then

closely matches our TDDMRG result. The energy difference of the two main Lorentzians leads to the oscillations whereas the Lorentzian shape leads to the exponential decay.

We gain additional insights by analyzing the response wavefunctions that contribute to the peaks (see Eq. (7) and Supplementary Section S3.3). The hole densities for these wavefunctions are all localized at the 2-oxoethyl group (shown in Supplementary Fig. S4). The wavefunction at 14.5 eV has large contributions from IBOs 1, 3, 4, and cIBO-1, indicating that this peak is due to both 1h and the 2h1p states discussed in the previous paragraph. In contrast, the wavefunction at 35.5 eV has large contributions from IBOs 1 and 4 only, hence no 2h1p configurations contribute to this peak. This discussion not only shows that IBOs can be used to analyze ionization spectra, but also that, remarkably, only the few IBOs shown in Fig. 4 are necessary to analyze a breakdown of the molecular orbital picture.

2. Furfural

Following a setting similar to that in phenylacetaldehyde, here we compare charge migration dynamics in furfural, where the initial hole is either a π C=O orbital (dubbed π dynamics) or a σ C=O orbital (dubbed σ dynamics). Unlike phenylacetaldehyde, furfural is planar, and the carbonyl group is π -conjugated with the furyl group. We have already studied furfural in Ref. [55] in terms of natural orbitals and dipole moments. Here, we use our IBOs, which provide a much more straightforward analysis and more insights.

Snapshots of the hole density for the π dynamics are shown in Fig. 7(a). As the molecule is fully π conjugated, the initial π hole rapidly migrates into the ring, which starts within the first 0.2 fs. This is more clearly visible through the IBO occupancies shown in Fig. 7(c). The π -conjugated IBOs 2-4 in the furyl ring quickly become populated, which is due to conjugation of these orbitals with the initial hole. Note that these orbitals have the same a'' symmetry and no σ -type orbitals with a' symmetry become populated during the π dynamics. A closer inspection of Fig. 7(c) shows that the hole occupancy first increases rapidly for the furyl C=C π IBO-2, followed by a similar but slightly delayed increase for IBO-3, which is the farthest away from the initial hole. At later times, the furyl oxygen p orbital also gains hole occupancy. However, next to the IBO occupancies, a full analysis also needs to include the negative occupancies of the antibonding cIBOs localized at the same bond as the bonding IBOs, which correspond to active 2h1p configurations and weaken a chemical bond. Adding the IBO and cIBO occupancies leads to an effective bond occupancy. These occupancies are shown in Fig. 7(d) and reveal a semi-stepwise migration to the different orbitals. We have seen a similar type of migration in the π dynamics of phenylacetaldehyde; c.f. Fig. 4(e).

Like our analysis of chloroacetylene in Section III A 1, the π dynamics can be understood in terms of Lewis structures and curly arrows; see Fig. 7(e). While helpful, such a curly-arrow mechanism of course only provides a rough qualitative understanding of the dynamics. It is difficult to extend curly-

arrow mechanisms to more complex migrations that display symmetry effects, strong entanglement and/or wavepacket bifurcations.

Snapshots of the hole density for the σ dynamics are shown in Fig. 7(b). Surprisingly, despite the vastly different initial states of the σ and π dynamics, within 0.484 fs, parts of the σ dynamics resemble the π dynamics. This is more clearly seen in the IBO analysis in panel (c); compare the occupancies of the π IBOs 2-4, and that of the cIBOs 1-3. All of these have a'' symmetry whereas the initial σ hole has a' symmetry. Hence, while the hole shape in the π dynamics remains unchanged, the hole in the σ dynamics changes to that of a π type as the hole enters the furyl group. Note the absence of active σ orbitals within the ring in Fig. 7(c). As the migration into the π furyl orbitals is the main mechanism, the σ dynamics is less efficient than the π dynamics and the total sum of the furyl IBO occupancies reaches a maximum value of only 0.60 for the σ dynamics, compared to 0.89 for the π dynamics.

As in phenylacetaldehyde in Section III B 1, the furyl π holes that appear in the σ dynamics are accompanied by strongly negative occupancies of antibonding cIBOs and a quasiexponential decay of key IBOs, e.g. IBO-7 in Fig. 7(c). Thus, also the furfural σ dynamics exhibits a breakdown of the MO picture and 2h1p configurations transfer the dominant hole character to orbitals of different symmetry. However, in contrast to phenylacetaldehyde, the migration into the ring is mediated through π conjugation rather than hyperconjugation.

C. Conformer effects

In Section III B, we have shown that both global and local symmetries can play a pivotal role in determining how the hole shape changes as it migrates through the molecule. So far, all molecules studied have global symmetry. What if the molecule has local symmetries but no global symmetry? To address this for a particular scenario, we study two C_1 -symmetric conformers of 3-fluoro-2-methylpropanal, namely the synclinal one (sc-3-fluoro-2-methylpropanal, dubbed SC), and the synperiplanar one (sp-3-fluoro-2-methylpropanal, dubbed SP); see Fig. 8 (a) and (b) for their geometries. SP is the global minimum, and SC is about 3.1 kJ/mol higher in energy. The conformers primarily differ in the placement of fluorine, whose lone pairs and high electronegativity can significantly affect charge migration. We will show below that the placement of fluorine can be crucial for efficient charge migration and thus suggest design principles for optimal charge migration.

For both conformers, our simulations start with a hole in the π bond of C=O. In Fig. 8(a) and (b) we show snapshots of the hole density for SC and SP, respectively. Unlike in our previous studies, we here only show the hole densities projected into the dominant IBO space, which facilitate the analysis.¹⁴⁶ As both conformers have the same initial hole, the conformer effect is not large during the initial dynamics but becomes larger at later times. Particularly, the hole density snapshots indicate that dominant changes in the charge migration start to appear at ~ 0.7 fs. After ~ 1 fs, the initial hole in SP becomes almost

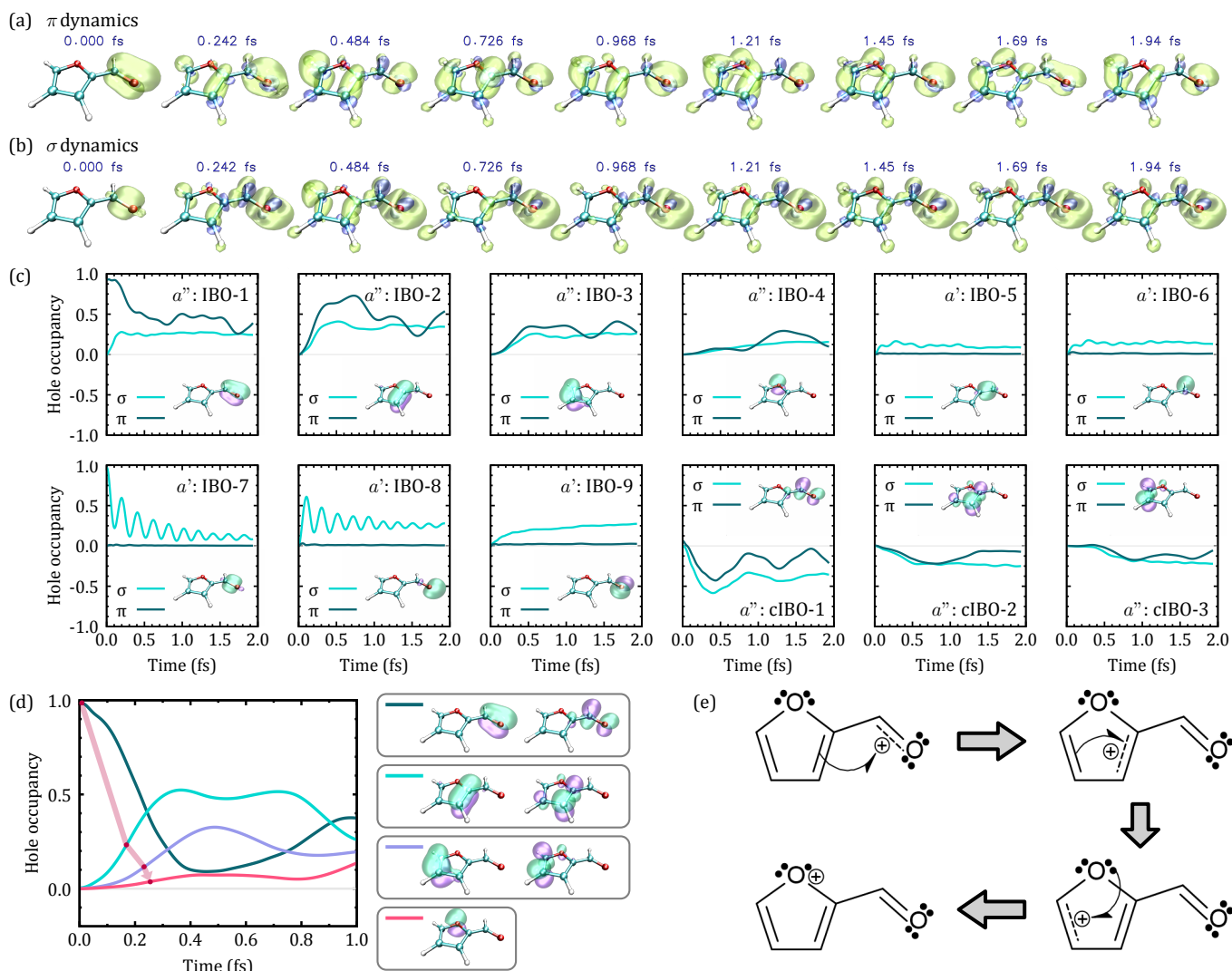


Figure 7: Charge migration analysis of furfural. (a, b) Hole density snapshots for the π and σ dynamics, respectively. The color code is the same as that in Fig. 2(a). (c) Dominant IBO hole occupancies. The IBO associated with each hole occupancy and its irrep label are shown in each panel. (d) Summed hole occupancies of the dominant IBOs and the corresponding cIBOs within the first 1 fs during the π dynamics. The red arrow suggests the movement of hole. (e) Curly arrow mechanism demonstrating the initial hole migration; compare with the red arrow in panel (d).

completely drained out. Hence, the placement of fluorine in SP leads to a more enhanced charge migration, compared to SC. The IBO hole occupancies provide more details and are shown in Fig. 8(c). The charge migration efficiency is clearly seen from IBO-1, whose occupancy starts close to 1 and for SP reaches a minimum of 0.090, whereas for SC it only reaches 0.26 for the time range studied.

The enhanced charge migration in SP can be explained by realizing the existence of a quasi-plane in the molecule formed by the numbered atoms in Fig. 8(d). This quasi-plane facilitates hyperconjugative interactions between orbitals/bonds connected to the plane: as shown in panels (b) and (c), the hole migrates from its initial location on the C=O π IBO-1 to the C₃-C₆ σ IBO-2 before finally arriving at the F atom's p lone-pair IBO-8. This stepwise migration is enabled by hyper-

conjugation on the quasi-plane, first between IBO-1 and IBO-2 and then between IBO-2 and IBO-8, which are shown in panel (e).

The local symmetry of the initial hole relative to this quasi-plane explains why bonds that are aligned parallel to the quasi-plane are inactive during the dynamics. For example, note that the C₂-C₃ σ IBO (not shown) is not active, as that orbital has a different local symmetry and thus cannot interact with IBO-1. Other examples are IBOs 3 and 7.

The above mechanism in SP cannot easily occur in SC because a similar quasi-plane with well-aligned orbitals that includes the F atom's occupied orbitals does not exist. There is some interaction between IBO-1 and SC IBO-7, which explains the occupancy of IBO-7. However, these two IBOs are not fully aligned with each other, which reduces their interac-

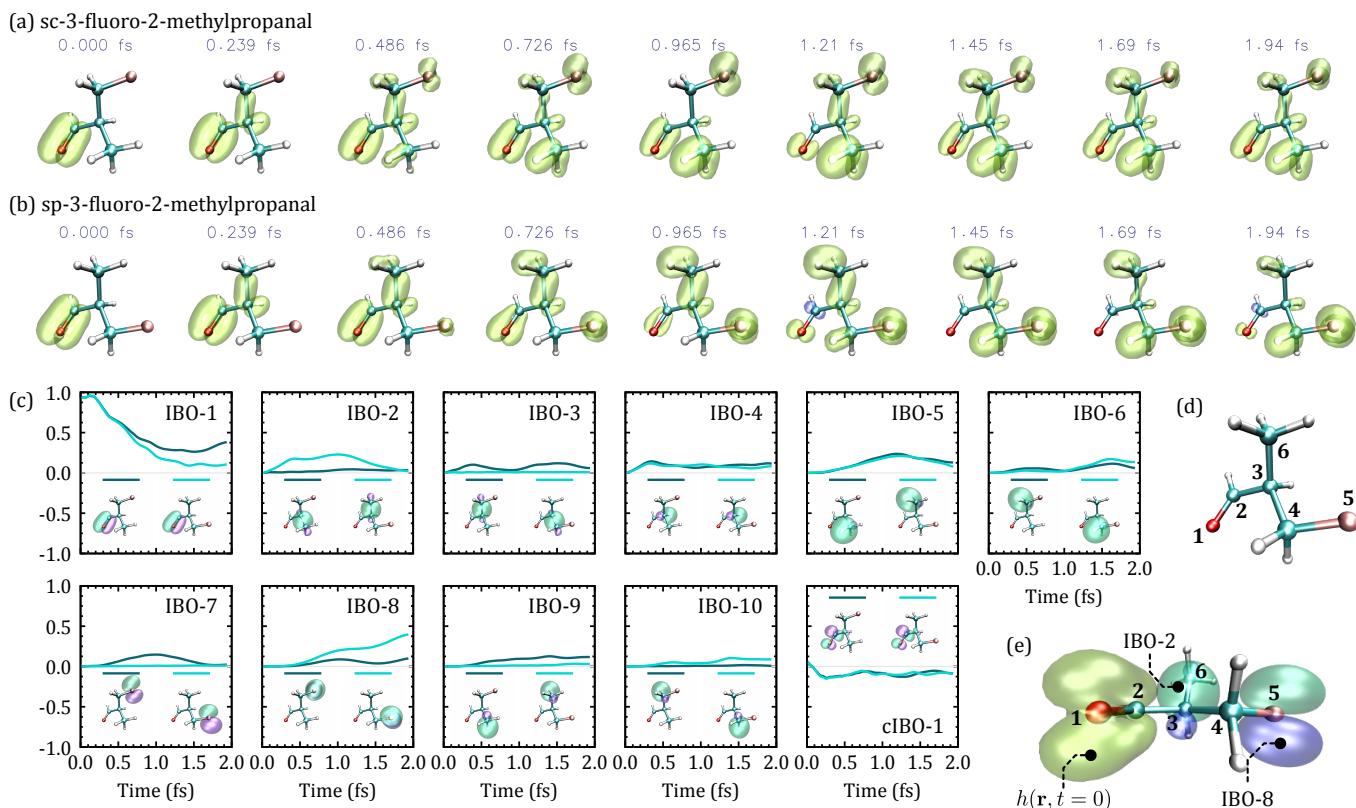


Figure 8: Charge migration analysis of sc-3-fluoro-2-methylpropanal. (a, b) Hole density snapshots sc-3-fluoro-2-methylpropanal (SC) and sp-3-fluoro-2-methylpropanal (SP), respectively. Note that only the densities projected into the dominant IBO space are shown. (c) Dominant IBO hole occupancies. The IBOs of the two conformers associated with each hole occupancy are shown in each panel. (d) Structure of SP highlighting the numbered atoms that define a quasi-plane and are essential for the charge migration. (e) Same as (d) but viewed at an angle that reveals the quasi-plane that connects the initial hole with IBOs 2 and 8.

tions.

While the migration toward the F atom differs markedly between the two conformers, we observe some similarities in other migration paths: the occupancy curves of cIBO-1, IBOs 4-6, and that of SC/SP IBOs 9/10 are very similar for both conformers. These IBOs are associated to migrations to other parts of the molecule, e.g. the hydrogen atoms. The similarity between the two conformers is due to the same type of initial dynamics, which is not affected by the placement of the F atom at the other end of the molecule.

Our results on SC and SP have demonstrated an interplay between initial hole symmetry, location of a functional group with lone pairs, and geometry in enhancing charge migration, and thus will be useful in the search effort of molecules that exhibit a clear charge migration signal. As the dynamics involve both σ , π , and p orbitals, they also present an example of the underlying similarity between conjugation and hyperconjugation⁹⁶ in the context of electron dynamics.

IV. CONCLUSIONS

In this work, we introduced a new way of analyzing charge migration dynamics that is based on mapping the hole density and related quantities to an extension of intrinsic bond orbitals (IBOs). This extension includes antibonding orbitals and leads to a very compact representation of the essentials of the real-time many-body quantum dynamics, even in challenging cases such as correlated inner-valence ionized wavefunction. The real-valued and time-independent nature of IBOs makes them particularly convenient to use for time-dependent simulations. Our simulations were based on an efficient setup of the time-dependent density matrix renormalization group (TDDMRG), which allowed us to simulate charge migration in molecules as large as phenylacetaldehyde with 45 fully correlated electrons in 50 orbitals.

IBOs bridge quantum mechanics with chemical concepts, and, in our case, enabled us to not only connect IBOs to established quantities in charge migration such as hole configurations, but also to understand complex charge migration in terms of through-bond interactions such as hyperconjugation and Lewis structures. We demonstrated this capability for various molecules, with a focus on how ionization from orbitals

of various shapes affect the charge migration. For example, we showed that in phenylacetaldehyde a sudden ionization at the carbonyl group leads to a migration into the σ bonds of the phenyl ring regardless of whether the initial hole has a π or a σ shape. We found that through-bond and through-space hyperconjugation interactions between different IBOs of similar local symmetry are responsible for this surprising effect. We also observed a rapid change of character from a σ hole to a π hole at the carbonyl bond, which we explained by connecting antibonding extensions of IBOs to excited two-hole one-particle (2h1p) configurations that couple orbitals with π and σ symmetries.

In contrast to phenylacetaldehyde, in furfural we found that charge at the carbonyl group migrates into the π bonds of the formyl group, regardless of whether the ionization created a π or σ hole at the carbonyl group. The π -hole-initiated migration is driven by a full conjugation of the π orbitals throughout the molecule, while the σ -hole-initiated migration is mediated by excited 2h1p configurations. Taking advantage of the straightforward mapping of IBOs to Lewis structures, we also demonstrated how an IBO analysis leads to a qualitative mechanism in terms of curly arrows for charge migrations without strong wavefunction bifurcations and interference effects.

Lastly, we used our extension of IBOs to explain different charge migration efficiencies of two conformers of 3-fluoro-2-methylpropanal. The localized character of the IBOs dramatically sped up this analysis. We found that, for one conformer, the charge migration is facilitated by through-space interactions of three key IBOs that form a quasi-plane. This leads to an almost complete drain of the initial hole, in contrast to the other conformer, where the IBOs are aligned less favorably. This illustrates a potential way to find molecules and functional groups with high charge migration efficiency, which is crucial for clear experiments. As such, we believe that the present work might help in realizing future experiments, and by extension, ultrafast control of chemical reactions.

While we focused on charge migration, the proposed IBO analysis can be extended to understand not only other types of nonequilibrium real-time molecular dynamics but also time-independent quantities such as response functions in ionization spectra, which we briefly demonstrated. Importantly, IBOs are not restricted to DMRG wavefunctions but can be combined with other quantum chemistry methods, including density functional theory.

ASSOCIATED CONTENT

Supporting Information available. Details on the used geometries, fitting procedure of the n -state model, and conformers; natural charge orbital analysis of the σ , π , and p dynamics, additional hole density snapshots of the p dynamics, and Green’s function analysis of the σ dynamics in phenylacetaldehyde; total hole occupancies in the phenyl and furyl rings; snapshots of the unprojected hole densities of the 3-fluoro-2-methylpropanal conformers; convergence studies for all dynamics.

Table II: TDDMRG propagation parameters. D_{prelim} and D are the bond dimensions for the preliminary and main TDDMRG propagations, respectively. The former is used for selecting the CAS orbitals.

| System / dynamics | D_{prelim} | D | Active space | $\Delta t/\text{as}$ |
|---------------------------|---------------------|------|---------------|----------------------|
| chloroacetylene | N/A | 1000 | CAS(15e, 41o) | 0.968 |
| chlorobutadiyne | 150 | 700 | CAS(23e, 45o) | 0.605 |
| phenylacetaldehyde | 100 | 500 | CAS(45e, 50o) | 0.484 |
| furfural (π) | 200 | 500 | CAS(35e, 40o) | 0.968 |
| furfural (σ) | 200 | 500 | CAS(35e, 40o) | 0.484 |
| 3-fluoro-2-methylpropanal | 150 | 500 | CAS(35e, 40o) | 0.726 |

ACKNOWLEDGMENTS

This work was supported by the U.S. Department of Energy, Office of Science, Office of Basic Energy Sciences under Award Number DE-SC0026361 (Green’s function computations, simulation analysis, Lewis structures), by the donors of American Chemical Society Petroleum Research Fund via grant no. 67511-DNI6 (IBO procedure, TD-DMRG simulations), and through computational time on the Pinnacles/CENVAL-ARC cluster at the Cyberinfrastructure and Research Technologies (CIRT) at University of California, Merced, supported by NSF Grants No. 2346744 and 2019144.

Appendix A: Computational details

Our TDDMRG implementation is based on the BLOCK2^{107,147} and PYSCEF^{148–150} codes. We follow our recently established guidelines for efficient TDDMRG charge migration simulations.⁵⁵ To enforce the spin SU(2) symmetry of open-shell wavefunctions resulting from ionization, we use a spin-adapted MPS. This leads to a slightly different basis than that given in Eq. (1), which only supports particle-number U(1) symmetry. Based on the findings in our previous work,⁵⁵ we use singlet-embedding for enforcing the nonzero total spin within the spin-adapted MPS, that is, the nonzero spin state is embedded in a state that has a total spin of zero.^{151,152} To propagate the complex-valued wavefunction, we use a fully complex MPS representation, i.e., all matrices $\mathbf{M}^{\sigma_i}(t)$ in Eq. (1) are complex-valued. The individual MPS matrices are propagated using the short iterative Lanczos algorithm¹⁵³ with a relative convergence tolerance of 5×10^{-6} . The main TDDMRG propagation parameters are outlined in Table II. See Supplementary Section S6 for convergence studies.

We use 6-31G basis set^{154,155} for all molecules except for chloroacetylene and chlorobutadiyne, for which we use the def2-SV(P) basis set.¹⁵⁶ All simulations use the frozen core approximation. The geometries were optimized using density functional theory (see Supplementary Section S1). For phenylacetaldehyde, the particular conformer is not the global minimum (other conformers that are 2.7 kJ/mol lower in energy exist), but it is accessible at room temperature.

To select the active orbitals for the CAS, we use our pro-

cedures developed in Ref. [55]. In short, we select the active orbitals for the dynamics from the dominant orbitals of both the reduced density matrix (RDM) of the neutral molecule's ground state and, in addition, from the time-averaged hole density matrix of a preliminary TDDMRG simulation using all orbitals and a small bond dimension D_{prelim} shown in Table II. To improve the DMRG efficiency, the selected orbitals are then split-localized using Pipek-Mezey localization.⁸¹ We employ these hole-DM-selected orbitals for all molecules except for chloroacetylene, for which we use split-localized Hartree-Fock orbitals and the full orbital space. Note that these orbitals used for the TDDMRG simulations are not IBOs. The IBO analysis is done through a change of basis.

For all molecules except chloroacetylene, we use the annihilation operator \hat{a}_k of a particular IBO $|k\rangle$ to create a localized initial hole. For chloroacetylene, we create the initial hole from an equal-weight superposition of Hartree-Fock HOMO and HOMO-1, which leads to a p lone-pair orbital on Cl. We compute restricted-Hartree-Fock-based IBOs using the implementation in PYSCF, which differs slightly from the original IBO procedure outlined in Ref. [86]. We compute the IBOs by localizing the MOs without directly enforcing symmetry, save for phenylacetaldehyde, where we localize the MOs within each irrep of the C_s point group. This makes the IBOs less localized but facilitates the charge migration analysis.

For the hole density and natural orbital plots, we use isosurface values of ± 0.006 , while for the IBOs, this value is ± 0.06 for all molecules except for furfural, which is ± 0.08 .

The ionization potentials of the states in the σ , π , and p dynamics of phenylacetaldehyde in Section III B 1 are 34.0 eV, 15.6 eV, and 14.9 eV, respectively. For furfural, the ionization potentials are 15.6 eV and 33.6 eV for the π dynamics and σ dynamics, respectively. We note that the energy of the σ dynamics for both molecules is higher than the second ionization potential, which means that some influence from Auger-Meitner decay to this dynamics should be expected at times longer than our simulation time.¹⁵⁷

The Green's function computations for phenylacetaldehyde in Section III B 1 are based on a bond dimension of $D = 550$, use a final relative convergence tolerance of 10^{-8} , a maximal sweep number of 8, and a linear solver tolerance of 10^{-6} . To steer the optimization problem out of local minima, we use noise on the order of 10^{-5} for the first 4 sweeps.

REFERENCES

- M. Nisoli, P. Decleva, F. Calegari, A. Palacios, and F. Martín, "Attosecond electron dynamics in molecules," *Chem. Rev.* **117**, 10760–10825 (2017).
- M. J. J. Vrakking and F. Lepine, *Attosecond Molecular Dynamics* (The Royal Society of Chemistry, 2018).
- A. Palacios and F. Martín, "The quantum chemistry of attosecond molecular science," *Wiley Interdiscip. Rev.: Comput. Mol. Sci.* **10**, e1430 (2020).
- I. C. D. Merritt, D. Jacquemin, and M. Vacher, "Attochemistry: Is controlling electrons the future of photochemistry?" *J. Phys. Chem. Lett.* **12**, 8404–8415 (2021).
- E. P. Månsson, S. De Camillis, M. C. Castrovilli, M. Galli, M. Nisoli, F. Calegari, and J. B. Greenwood, "Ultrafast dynamics in the DNA building blocks thymidine and thymine initiated by ionizing radiation," *Phys. Chem. Chem. Phys.* **19**, 19815–19821 (2017).
- P. Swiderek, "Fundamental Processes in Radiation Damage of DNA," *Angew. Chem. Int. Ed.* **45**, 4056–4059 (2006).
- R. Weinkauff, P. Schanen, A. Metsala, E. W. Schlag, M. Bürgle, and H. Kessler, "Highly efficient charge transfer in peptide cations in the gas phase: Threshold effects and mechanism," *J. Phys. Chem.* **100**, 18567–18585 (1996).
- R. Weinkauff, E. W. Schlag, T. J. Martinez, and R. D. Levine, "Nonstationary electronic states and site-selective reactivity," *J. Phys. Chem. A* **101**, 7702–7710 (1997).
- F. Remacle, R. Levine, and M. Ratner, "Charge directed reactivity: a simple electronic model, exhibiting site selectivity, for the dissociation of ions," *Chem. Phys. Lett.* **285**, 25–33 (1998).
- F. Remacle, R. D. Levine, E. W. Schlag, and R. Weinkauff, "Electronic control of site selective reactivity: A model combining charge migration and dissociation," *J. Phys. Chem. A* **103**, 10149–10158 (1999).
- W. Cui, M. S. Thompson, and J. P. Reilly, "Pathways of peptide ion fragmentation induced by vacuum ultraviolet light," *J. Am. Soc. Mass Spectrom.* **16**, 1384–1398 (2005).
- F. Remacle and R. D. Levine, "Probing ultrafast purely electronic charge migration in small peptides," *Z. Phys. Chem.* **221**, 647–661 (2007).
- J. P. Reilly, "Ultraviolet photofragmentation of biomolecular ions," *Mass Spectrom. Rev.* **28**, 425–447 (2009).
- F. Remacle and R. D. Levine, "Charge migration and control of site selective reactivity: The role of covalent and ionic states," *J. Chem. Phys.* **110**, 5089–5099 (1999).
- M. F. Kling, P. von den Hoff, I. Znakovskaya, and R. de Vivie-Riedle, "(Sub-)femtosecond control of molecular reactions via tailoring the electric field of light," *Phys. Chem. Chem. Phys.* **15**, 9448–9467 (2013).
- N. V. Golubev and A. I. Kuleff, "Control of charge migration in molecules by ultrashort laser pulses," *Phys. Rev. A* **91**, 051401 (2015).
- V. D. Nikolay V. Golubev and A. I. Kuleff, "Quantum control with smoothly varying pulses: general theory and application to charge migration," *J. Mod. Opt.* **64**, 1031–1041 (2017).
- L. Cederbaum and J. Zobeley, "Ultrafast charge migration by electron correlation," *Chem. Phys. Lett.* **307**, 205–210 (1999).
- J. Breidbach and L. S. Cederbaum, "Universal attosecond response to the removal of an electron," *Phys. Rev. Lett.* **94**, 033901 (2005).
- F. Remacle and R. D. Levine, "An electronic time scale in chemistry," *Proc. Natl. Acad. Sci. USA* **103**, 6793–6798 (2006).
- P. B. Corkum and F. Krausz, "Attosecond science," *Nat. Phys.* **3**, 381–387 (2007).
- S. R. Leone, C. W. McCurdy, J. Burgdörfer, L. S. Cederbaum, Z. Chang, N. Dudovich, J. Feist, C. H. Greene, M. Ivanov, R. Kienberger, *et al.*, "What will it take to observe processes in 'real time'?" *Nat. Photonics* **8**, 162–166 (2014).
- L. Belshaw, F. Calegari, M. J. Duffy, A. Trabattani, L. Poletto, M. Nisoli, and J. B. Greenwood, "Observation of ultrafast charge migration in an amino acid," *J. Phys. Chem. Lett.* **3**, 3751–3754 (2012).
- F. Calegari, D. Ayuso, A. Trabattani, L. Belshaw, S. D. Camillis, S. Anumula, F. Frassetto, L. Poletto, A. Palacios, P. Decleva, J. B. Greenwood, F. Martín, and M. Nisoli, "Ultrafast electron dynamics in phenylalanine initiated by attosecond pulses," *Science* **346**, 336–339 (2014).
- F. Calegari, D. Ayuso, A. Trabattani, L. Belshaw, S. De Camillis, F. Frassetto, L. Poletto, A. Palacios, P. Decleva, J. B. Greenwood, F. Martín, and M. Nisoli, "Ultrafast charge dynamics in an amino acid induced by attosecond pulses," *IEEE J. Sel. Top. Quantum Electron.* **21**, 1–12 (2015).
- P. M. Kraus, B. Mignolet, D. Baykusheva, A. Rupenyan, L. Horný, E. F. Penka, G. Grassi, O. I. Tolstikhin, J. Schneider, F. Jensen, L. B. Madsen, A. D. Bandrauk, F. Remacle, and H. J. Wörner, "Measurement and laser control of attosecond charge migration in ionized iodoacetylene," *Science* **350**, 790–795 (2015).
- V. Despré, A. Marciniak, V. Loriot, M. C. E. Galbraith, A. Rouzée, M. J. J. Vrakking, F. Lépine, and A. I. Kuleff, "Attosecond hole migration in benzene molecules surviving nuclear motion," *J. Phys. Chem. Lett.* **6**, 426–431 (2015).
- M. Vacher, L. Steinberg, A. J. Jenkins, M. J. Bearpark, and M. A. Robb, "Electron dynamics following photoionization: Decoherence due to the nuclear-wave-packet width," *Phys. Rev. A* **92**, 040502 (2015).
- V. Despré, A. Marciniak, V. Loriot, M. C. E. Galbraith, A. Rouzée, M. J. J. Vrakking, F. Lépine, and A. I. Kuleff, "Attosecond hole migration in ben-

- zene molecules surviving nuclear motion,” *J. Phys. Chem. Lett.* **6**, 426–431 (2015).
- ³⁰C. Arnold, O. Vendrell, and R. Santra, “Electronic decoherence following photoionization: Full quantum-dynamical treatment of the influence of nuclear motion,” *Phys. Rev. A* **95**, 033425 (2017).
- ³¹M. Vacher, M. J. Bearpark, M. A. Robb, and J. a. P. Malhado, “Electron dynamics upon ionization of polyatomic molecules: Coupling to quantum nuclear motion and decoherence,” *Phys. Rev. Lett.* **118**, 083001 (2017).
- ³²V. Despré, N. V. Golubev, and A. I. Kuleff, “Charge migration in propiolic acid: A full quantum dynamical study,” *Phys. Rev. Lett.* **121**, 203002 (2018).
- ³³H. Ma, J. Manz, H. Wang, Y. Yan, and Y. Yang, “Ultrafast laser induced charge migration with de- and re-coherences in polyatomic molecules: A general method with application to pyrene,” *J. Chem. Phys.* **158**, 124306 (2023).
- ³⁴A. Scheidegger, N. V. Golubev, and J. Vaníček, “How to find molecules with long-lasting charge migration?” *Chimia* **77**, 201–205 (2023).
- ³⁵K. Chordiya, V. Despré, B. Nagyllés, F. Zeller, Z. Diveki, A. I. Kuleff, and M. U. Kahaly, “Photo-ionization initiated differential ultrafast charge migration: impacts of molecular symmetries and tautomeric forms,” *Phys. Chem. Chem. Phys.* **25**, 4472–4480 (2023).
- ³⁶D. Haase, J. Manz, and J. C. Tremblay, “Attosecond charge migration can break electron symmetry while conserving nuclear symmetry,” *J. Phys. Chem. A* **124**, 3329–3334 (2020).
- ³⁷S. Giri, G. Dixit, and J. C. Tremblay, “Attosecond charge migration in heterocyclic five-membered rings,” *Eur. Phys. J.: Spec. Top.* **232**, 1935–1943 (2023).
- ³⁸J. C. Tremblay, A. Blanc, P. Krause, S. Giri, and G. Dixit, “Probing Electronic Symmetry Reduction during Charge Migration via Time-Resolved X-Ray Diffraction,” *Chem. Phys. Chem.* **24**, e202200463 (2023).
- ³⁹S. Lünemann, A. I. Kuleff, and L. S. Cederbaum, “Ultrafast charge migration in 2-phenylethyl-n,n-dimethylamine,” *Chem. Phys. Lett.* **450**, 232–235 (2008).
- ⁴⁰A. I. Kuleff, S. Lünemann, and L. S. Cederbaum, “Electron-correlation-driven charge migration in oligopeptides,” *Chem. Phys.* **414**, 100–105 (2013).
- ⁴¹A. Bruner, S. Hernandez, F. Mauger, P. M. Abanador, D. J. LaMaster, M. B. Gaarde, K. J. Schafer, and K. Lopata, “Attosecond Charge Migration with TDDFT: Accurate Dynamics from a Well-Defined Initial State,” *J. Phys. Chem. Lett.* **8**, 3991–3996 (2017).
- ⁴²D. Jia, J. Manz, B. Paulus, V. Pohl, J. C. Tremblay, and Y. Yang, “Quantum control of electronic fluxes during adiabatic attosecond charge migration in degenerate superposition states of benzene,” *Chem. Phys.* **482**, 146–159 (2017).
- ⁴³M. Lara-Astiaso, A. Palacios, P. Declava, I. Tavernelli, and F. Martín, “Role of electron-nuclear coupled dynamics on charge migration induced by attosecond pulses in glycine,” *Chem. Phys. Lett.* **683**, 357–364 (2017).
- ⁴⁴K. A. Hamer, F. Mauger, A. S. Folorunso, K. Lopata, R. R. Jones, L. F. DiMauro, K. J. Schafer, and M. B. Gaarde, “Characterizing particle-like charge-migration dynamics with high-order harmonic sideband spectroscopy,” *Phys. Rev. A* **106**, 013103 (2022).
- ⁴⁵K. A. Hamer, A. S. Folorunso, K. Lopata, K. J. Schafer, M. B. Gaarde, and F. Mauger, “Tracking charge migration with frequency-matched strobospectroscopy,” *J. Phys. Chem. A* **128**, 20–27 (2024).
- ⁴⁶C. Guiot du Doignon, R. Sinha-Roy, F. Rabilloud, and V. Despré, “Correlation-driven charge migration triggered by infrared multi-photon ionization,” *Chem. Sci.* **16**, 16729–16736 (2025).
- ⁴⁷J. Breidbach and L. S. Cederbaum, “Migration of holes: Formalism, mechanisms, and illustrative applications,” *J. Chem. Phys.* **118**, 3983–3996 (2003).
- ⁴⁸J. Breidbach and L. S. Cederbaum, “Migration of holes: Numerical algorithms and implementation,” *J. Chem. Phys.* **126**, 034101 (2007).
- ⁴⁹A. S. Folorunso, A. Bruner, F. Mauger, K. A. Hamer, S. Hernandez, R. R. Jones, L. F. DiMauro, M. B. Gaarde, K. J. Schafer, and K. Lopata, “Molecular modes of attosecond charge migration,” *Phys. Rev. Lett.* **126**, 133002 (2021).
- ⁵⁰A. S. Folorunso, F. Mauger, K. A. Hamer, D. D. Jayasinghe, I. S. Wahyutama, J. R. Ragains, R. R. Jones, L. F. DiMauro, M. B. Gaarde, K. J. Schafer, and K. Lopata, “Attochemistry regulation of charge migration,” *J. Phys. Chem. A* **127**, 1894–1900 (2023).
- ⁵¹T. Hua, L. Kurkowski, and K. Lopata, “The effect of core-hole shape on attosecond valence electron dynamics,” *J. Phys. Chem. A* **129**, 7742–7750 (2025).
- ⁵²K. A. Hamer, F. Mauger, K. Lopata, K. J. Schafer, and M. B. Gaarde, “Strong-field ionization with few-cycle, midinfrared laser pulses inducing a localized ionization followed by long-lasting charge migration in halogenated organic molecules,” *Phys. Rev. A* **111**, L011101 (2025).
- ⁵³D. Mendive-Tapia, M. Vacher, M. J. Bearpark, and M. A. Robb, “Coupled electron-nuclear dynamics: Charge migration and charge transfer initiated near a conical intersection,” *J. Chem. Phys.* **139**, 044110 (2013).
- ⁵⁴F. Khalili, M. Vafaei, D. Cho, and B. Shokri, “Charge migration in caffeine: A real-time time-dependent density functional theory study,” *Int. J. Quantum Chem.* **121**, e26754 (2021).
- ⁵⁵I. S. Wahyutama and H. R. Larsson, “Simulating real-time molecular electron dynamics efficiently using the time-dependent density matrix renormalization group,” *J. Chem. Theory Comput.* **20**, 9814–9831 (2024).
- ⁵⁶V. Pohl, G. Hermann, and J. C. Tremblay, “An open-source framework for analyzing N-electron dynamics. I. Multideterminantal wave functions,” *J. Comput. Chem.* **38**, 1515–1527 (2017).
- ⁵⁷G. Hermann, V. Pohl, G. Dixit, and J. C. Tremblay, “Probing Electronic Fluxes via Time-Resolved X-Ray Scattering,” *Phys. Rev. Lett.* **124**, 013002 (2020).
- ⁵⁸Y. Meng, H. Wang, Y. Zhang, and Y. Yang, “Ultrafast charge migration in ionized iodo-alkyne chain $I(CC)_nH^+$,” *AIP Adv.* **13**, 045301 (2023).
- ⁵⁹H. Wang, X. Ren, X. Ren, L. Xiao, S. Jia, and Y. Yang, “Coherences of charge migration increasing with molecular size: A case study for chloroalkyne ions $H(CC)_nCl^+$,” *Phys. Rev. Res.* **7**, L022003 (2025).
- ⁶⁰H. J. Wörner, C. A. Arrell, N. Banerji, A. Cannizzo, M. Chergui, A. K. Das, P. Hamm, U. Keller, P. M. Kraus, E. Liberatore, P. Lopez-Tarifa, M. Lucchini, M. Meuwly, C. Milne, J.-E. Moser, U. Rothlisberger, G. Smolentsev, J. Teuscher, J. A. van Bokhoven, and O. Wenger, “Charge migration and charge transfer in molecular systems,” *Struct. Dyn.* **4**, 061508 (2017).
- ⁶¹V. Despré and A. I. Kuleff, “Correlation-driven charge migration as an initial step of the dynamics in correlation bands,” *Phys. Rev. A* **106**, L021501 (2022).
- ⁶²D. T. Matselyukh, V. Despré, N. V. Golubev, A. I. Kuleff, and H. J. Wörner, “Decoherence and revival in attosecond charge migration driven by non-adiabatic dynamics,” *Nat. Phys.* **18**, 1206–1213 (2022).
- ⁶³D. Schwickert, M. Ruberti, P. Kolorenč, S. Usenko, A. Przystawik, K. Baev, I. Baev, M. Braune, L. Bocklage, M. K. Czwalińska, S. Deinert, S. Düsterer, A. Hans, G. Hartmann, C. Haunhorst, M. Kuhlmann, S. Palutke, R. Röhlberger, J. Rönsch-Schulenburg, P. Schmidt, S. Toleikis, J. Viefhaus, M. Martins, A. Knie, D. Kip, V. Averbukh, J. P. Marangos, and T. Laarmann, “Electronic quantum coherence in glycine molecules probed with ultrashort X-ray pulses in real time,” *Sci. Adv.* **8**, eabn6848 (2022).
- ⁶⁴F. Calegari and F. Martin, “Open questions in attochemistry,” *Commun. Chem.* **6**, 184 (2023).
- ⁶⁵V. Wanie, E. Bloch, E. P. Månsson, L. Colaizzi, S. Ryabchuk, K. Saraswathula, A. F. Ordóñez, D. Ayuso, O. Smirnova, A. Trabattini, *et al.*, “Capturing electron-driven chiral dynamics in UV-excited molecules,” *Nature* **630**, 109–115 (2024).
- ⁶⁶D. Haase, J. Manz, B. Paulus, J. Scherfützki, and J. C. Tremblay, “A simple approach to attosecond electronic chirality flips using triatomic molecules,” *Phys. Chem. Chem. Phys.* **28**, 5175–5180 (2026).
- ⁶⁷W. O. Kermack and R. Robinson, “LI.—An explanation of the property of induced polarity of atoms and an interpretation of the theory of partial valencies on an electronic basis,” *J. Chem. Soc. Trans.* **121**, 427–440 (1922).
- ⁶⁸K. Kitaura and K. Morokuma, “A new energy decomposition scheme for molecular interactions within the Hartree-Fock approximation,” *Int. J. Quantum Chem.* **10**, 325–340 (1976).
- ⁶⁹E. D. Glendenning, “Natural energy decomposition analysis: Explicit evaluation of electrostatic and polarization effects with application to aqueous clusters of alkali metal cations and neutrals,” *J. Am. Chem. Soc.* **118**, 2473–2482 (1996).
- ⁷⁰P. Su and H. Li, “Energy decomposition analysis of covalent bonds and intermolecular interactions,” *J. Chem. Phys.* **131**, 014102 (2009).
- ⁷¹P. Su, Z. Jiang, Z. Chen, and W. Wu, “Energy Decomposition Scheme Based on the Generalized Kohn-Sham Scheme,” *J. Phys. Chem. A* **118**, 2531–2542 (2014).
- ⁷²P. R. Horn, Y. Mao, and M. Head-Gordon, “Probing non-covalent interac-

- tions with a second generation energy decomposition analysis using absolutely localized molecular orbitals,” *Phys. Chem. Chem. Phys.* **18**, 23067–23079 (2016).
- ⁷³T. Lu and Q. Chen, “Simple, efficient, and universal energy decomposition analysis method based on dispersion-corrected density functional theory,” *J. Phys. Chem. A* **127**, 7023–7035 (2023).
- ⁷⁴Y. Liu, P. Kilby, T. J. Frankcombe, and T. W. Schmidt, “The electronic structure of benzene from a tiling of the correlated 126-dimensional wavefunction,” *Nat. Commun.* **11**, 1210 (2020).
- ⁷⁵Y. Liu, T. J. Frankcombe, and T. W. Schmidt, “The hitchhiker’s guide to the wave function,” *J. Phys. Chem. A* **126**, 979–991 (2022).
- ⁷⁶K. Boguslawski, P. Tecmer, Ö. Legeza, and M. Reiher, “Entanglement measures for single- and multireference correlation effects,” *J. Phys. Chem. Lett.* **3**, 3129–3135 (2012).
- ⁷⁷S. Szalay, G. Barcza, T. Szilvási, L. Veis, and Ö. Legeza, “The correlation theory of the chemical bond,” *Sci. Rep.* **7**, 2237 (2017).
- ⁷⁸L. Ding, G. Dünneweber, and C. Schilling, “Physical entanglement between localized orbitals,” *Quantum Sci. Technol.* **9**, 015005 (2023).
- ⁷⁹S. F. Boys, “Construction of some molecular orbitals to be approximately invariant for changes from one molecule to another,” *Rev. Mod. Phys.* **32**, 296–299 (1960).
- ⁸⁰C. Edmiston and K. Ruedenberg, “Localized atomic and molecular orbitals,” *Rev. Mod. Phys.* **35**, 457–464 (1963).
- ⁸¹J. Pipeke and P. G. Mezey, “A fast intrinsic localization procedure applicable for *ab initio* and semiempirical linear combination of atomic orbital wave functions,” *J. Chem. Phys.* **90**, 4916–4926 (1989).
- ⁸²M. S. Lee and M. Head-Gordon, “Polarized atomic orbitals for self-consistent field electronic structure calculations,” *J. Chem. Phys.* **107**, 9085–9095 (1997).
- ⁸³M. S. Lee and M. Head-Gordon, “Extracting polarized atomic orbitals from molecular orbital calculations,” *Int. J. Quantum Chem.* **76**, 169–184 (2000).
- ⁸⁴J. E. Subotnik, A. D. Dutoi, and M. Head-Gordon, “Fast localized orthonormal virtual orbitals which depend smoothly on nuclear coordinates,” *J. Chem. Phys.* **123**, 114108 (2005).
- ⁸⁵D. N. Laikov, “Intrinsic minimal atomic basis representation of molecular electronic wavefunctions,” *Int. J. Quantum Chem.* **111**, 2851–2867 (2011).
- ⁸⁶G. Knizia, “Intrinsic atomic orbitals: An unbiased bridge between quantum theory and chemical concepts,” *J. Chem. Theory Comput.* **9**, 4834–4843 (2013).
- ⁸⁷A. C. West, M. W. Schmidt, M. S. Gordon, and K. Ruedenberg, “A comprehensive analysis of molecule-intrinsic quasi-atomic, bonding, and correlating orbitals. I. Hartree-Fock wave functions,” *J. Chem. Phys.* **139**, 234107 (2013).
- ⁸⁸G. Knizia and J. E. M. N. Klein, “Electron flow in reaction mechanisms—revealed from first principles,” *Angew. Chem., Int. Ed.* **54**, 5518–5522 (2015).
- ⁸⁹L. Nunes dos Santos Comprido, J. E. M. N. Klein, G. Knizia, J. Kästner, and A. S. K. Hashmi, “The stabilizing effects in gold carbene complexes,” *Angew. Chem., Int. Ed.* **54**, 10336–10340 (2015).
- ⁹⁰Y.-H. Cheng, Y.-S. Ho, C.-J. Yang, C.-Y. Chen, C.-T. Hsieh, and M.-J. Cheng, “Electron Dynamics in Alkane C–H Activation Mediated by Transition Metal Complexes,” *J. Phys. Chem. A* **128**, 4638–4650 (2024).
- ⁹¹J. E. M. N. Klein and G. Knizia, “cPCET versus HAT: A Direct Theoretical Method for Distinguishing X–H Bond-Activation Mechanisms,” *Angew. Chem., Int. Ed.* **57**, 11913–11917 (2018).
- ⁹²A. Balakrishnan, W.-S. Chen, Y.-H. Cheng, K.-H. Wang, and M.-J. Cheng, “Unveiling Electron Dynamics in the Electrochemical Reduction of CO₂ to Methane on Copper,” *ChemPlusChem* **90**, e2500250 (2025).
- ⁹³C.-T. Hsieh, Y.-T. Tang, Y.-S. Ho, W.-K. Shao, and M.-J. Cheng, “Methane to Methanol Conversion over N-Doped Graphene Facilitated by Electrochemical Oxygen Evolution: A First-Principles Study,” *J. Phys. Chem. C* **127**, 308–318 (2023).
- ⁹⁴W. D. Derricotte and F. A. Evangelista, “Localized intrinsic valence virtual orbitals as a tool for the automatic classification of core excited states,” *J. Chem. Theory Comput.* **13**, 5984–5999 (2017).
- ⁹⁵T. A. Corry and P. J. O’Malley, “Localized Bond Orbital Analysis of the Bonds of O₂,” *J. Phys. Chem. A* **124**, 9771–9776 (2020).
- ⁹⁶I. V. Alabugin, G. dos Passos Gomes, and M. A. Abdo, “Hyperconjugation,” *Wiley Interdiscip. Rev.: Comput. Mol. Sci.* **9**, e1389 (2019).
- ⁹⁷A. Scheidegger, N. V. Golubev, and J. J. L. Vaníček, “Can increasing the size and flexibility of a molecule reduce decoherence and prolong charge migration?” *Proc. Natl. Acad. Sci. USA* **122**, e2501319122 (2025).
- ⁹⁸X. Li, N. Govind, C. Isborn, A. E. DePrince III, and K. Lopata, “Real-time time-dependent electronic structure theory,” *Chem. Rev.* **120**, 9951–9993 (2020).
- ⁹⁹G. K.-L. Chan and M. Head-Gordon, “Highly correlated calculations with a polynomial cost algorithm: A study of the density matrix renormalization group,” *J. Chem. Phys.* **116**, 4462–4476 (2002).
- ¹⁰⁰C. Lubich, T. Rohwedder, R. Schneider, and B. Vandereycken, “Dynamical Approximation by Hierarchical Tucker and Tensor-Train Tensors,” *SIAM J. Matrix Anal. Appl.* **34**, 470–494 (2013).
- ¹⁰¹C. Lubich, I. V. Oseledets, and B. Vandereycken, “Time integration of tensor trains,” *SIAM J. Numer. Anal.* **53**, 917–941 (2015).
- ¹⁰²J. Haegeman, C. Lubich, I. Oseledets, B. Vandereycken, and F. Verstraete, “Unifying time evolution and optimization with matrix product states,” *Phys. Rev. B* **94**, 165116 (2016).
- ¹⁰³S. Paeckel, T. Köhler, A. Swoboda, S. R. Manmana, U. Schollwöck, and C. Hubig, “Time-evolution methods for matrix-product states,” *Ann. Phys.* **411**, 167998 (2019).
- ¹⁰⁴L.-H. Frahm and D. Pfannkuche, “Ultrafast *ab initio* quantum chemistry using matrix product states,” *J. Chem. Theory Comput.* **15**, 2154–2165 (2019).
- ¹⁰⁵A. Baiardi, “Electron dynamics with the time-dependent density matrix renormalization group,” *J. Chem. Theory Comput.* **17**, 3320–3334 (2021).
- ¹⁰⁶H. Zhai and G. K.-L. Chan, “Low communication high performance *ab initio* density matrix renormalization group algorithms,” *J. Chem. Phys.* **154**, 224116 (2021).
- ¹⁰⁷H. Zhai, H. R. Larsson, S. Lee, Z.-H. Cui, T. Zhu, C. Sun, L. Peng, R. Peng, K. Liao, J. Tölle, J. Yang, S. Li, and G. K.-L. Chan, “Block2: A comprehensive open source framework to develop and apply state-of-the-art DMRG algorithms in electronic structure and beyond,” *J. Chem. Phys.* **159**, 234801 (2023).
- ¹⁰⁸H. R. Larsson, “A tensor network view of multilayer multiconfiguration time-dependent Hartree methods,” *Mol. Phys.* **122**, e2306881 (2024).
- ¹⁰⁹R. L. Martin, “Natural transition orbitals,” *J. Chem. Phys.* **118**, 4775–4777 (2003).
- ¹¹⁰A. I. Krylov, “From orbitals to observables and back,” *J. Chem. Phys.* **153**, 080901 (2020).
- ¹¹¹J. M. Herbert, “Visualizing and characterizing excited states from time-dependent density functional theory,” *Phys. Chem. Chem. Phys.* **26**, 3755–3794 (2024).
- ¹¹²A. J. Bovill, A. Abou Taka, H. Harb, and H. P. Hratchian, “Excitation/relaxation analysis of electronic transitions using difference density natural orbitals,” *J. Chem. Theory Comput.* **22**, 930–939 (2026).
- ¹¹³A. D. Dutoi, M. Wormit, and L. S. Cederbaum, “Ultrafast charge separation driven by differential particle and hole mobilities,” *J. Chem. Phys.* **134**, 024303 (2011).
- ¹¹⁴F. Langkabel, P. A. Albrecht, A. Bande, and P. Krause, “Making optical excitations visible – an exciton wavefunction extension to the time-dependent configuration interaction method,” *Chem. Phys.* **557**, 111502 (2022).
- ¹¹⁵T. Moitra, L. Konecny, M. Kadek, A. Rubio, and M. Repisky, “Accurate relativistic real-time time-dependent density functional theory for valence and core attosecond transient absorption spectroscopy,” *J. Phys. Chem. Lett.* **14**, 1714–1724 (2023).
- ¹¹⁶S. Upadhyay, X. Zheng, T. Wang, A. Shayit, J. Liu, D. Sun, and X. Li, “Chirality-driven magnetization emerges from relativistic four-current dynamics,” *APL Comput. Phys.* **2**, 016103 (2026).
- ¹¹⁷J. Wang, T. Driver, P. L. Franz, P. c. v. Kolorenč, E. Thierstein, R. R. Robles, E. Isele, Z. Guo, D. Cesar, O. Alexander, S. Beauvarlet, K. Borne, X. Cheng, L. F. DiMauro, J. Duris, J. M. Glowonia, M. Graßl, P. Hockett, M. Hoffman, A. Kamalov, K. A. Larsen, S. Li, X. Li, M.-F. Lin, R. Obaid, P. Rosenberger, P. Walter, T. J. A. Wolf, J. P. Marangos, M. F. Kling, P. H. Bucksbaum, A. Marinelli, and J. P. Cryan, “Probing electronic coherence between core-level vacancies at different atomic sites,” *Phys. Rev. X* **15**, 011008 (2025).
- ¹¹⁸R. Gordon, “Correlation functions for molecular motion,” in *Advances in Magnetic Resonance*, Advances in Magnetic and Optical Resonance, Vol. 3, edited by J. S. Waugh (Academic Press, 1968) pp. 1–42.
- ¹¹⁹D. J. Tannor, *Introduction to Quantum Mechanics: A Time-Dependent Perspective* (University Science Books, 2007).

- ¹²⁰E. Jeckelmann, "Dynamical density-matrix renormalization-group method," *Phys. Rev. B* **66**, 045114 (2002).
- ¹²¹E. Ronca, Z. Li, C. A. Jimenez-Hoyos, and G. K.-L. Chan, "Time-step targeting time-dependent and dynamical density matrix renormalization group algorithms with *ab initio* hamiltonians," *J. Chem. Theory Comput.* **13**, 5560–5571 (2017).
- ¹²²M. Rano and H. R. Larsson, "Computing excited eigenstates using exact Lanczos methods and tree tensor network states," *J. Chem. Phys.* **163**, 164110 (2025).
- ¹²³R. Manne and T. Åberg, "Koopmans' theorem for inner-shell ionization," *Chem. Phys. Lett.* **7**, 282–284 (1970).
- ¹²⁴B. Mignolet, R. D. Levine, and F. Remacle, "Localized electron dynamics in attosecond-pulse-excited molecular systems: Probing the time-dependent electron density by sudden photoionization," *Phys. Rev. A* **86**, 053429 (2012).
- ¹²⁵G. Grell, S. I. Bokarev, B. Winter, R. Seidel, E. F. Aziz, S. G. Aziz, and O. Kühn, "Multi-reference approach to the calculation of photoelectron spectra including spin-orbit coupling," *J. Chem. Phys.* **143**, 074104 (2015).
- ¹²⁶V. Kochetov and S. I. Bokarev, "RhoDyn: A ρ -TD-RASCI Framework to Study Ultrafast Electron Dynamics in Molecules," *J. Chem. Theory Comput.* **18**, 46–58 (2022).
- ¹²⁷B. T. Pickup, "On the theory of fast photoionization processes," *Chem. Phys.* **19**, 193–208 (1977).
- ¹²⁸L. S. Cederbaum, W. Domcke, J. Schirmer, and W. V. Niessen, "Correlation effects in the ionization of molecules: Breakdown of the molecular orbital picture," in *Advances in Chemical Physics* (John Wiley & Sons, Ltd, 1986) pp. 115–159.
- ¹²⁹K. R. Roby, "Quantum theory of chemical valence concepts," *Mol. Phys.* **27**, 81–104 (1974).
- ¹³⁰R. Heinzmann and R. Ahlrichs, "Population analysis based on occupation numbers of modified atomic orbitals (MAOs)," *Theor. Chim. Acta* **42**, 33–45 (1976).
- ¹³¹S. Iwata, "Valence type vacant orbitals for configuration interaction calculations," *Chem. Phys. Lett.* **83**, 134–138 (1981).
- ¹³²K. Ruedenberg, M. W. Schmidt, and M. M. Gilbert, "Are atoms intrinsic to molecular electronic wavefunctions? II. Analysis of FORS orbitals," *Chem. Phys.* **71**, 51–64 (1982).
- ¹³³W. C. Lu, C. Z. Wang, M. W. Schmidt, L. Bytautas, K. M. Ho, and K. Ruedenberg, "Molecule intrinsic minimal basis sets. I. Exact resolution of *ab initio* optimized molecular orbitals in terms of deformed atomic minimal-basis orbitals," *J. Chem. Phys.* **120**, 2629–2637 (2004).
- ¹³⁴J. Ivanic, G. J. Atchity, and K. Ruedenberg, "Intrinsic local constituents of molecular electronic wave functions. I. Exact representation of the density matrix in terms of chemically deformed and oriented atomic minimal basis set orbitals," *Theor. Chem. Acc.* **120**, 281–294 (2008).
- ¹³⁵J. S. Steen, G. Knizia, and J. E. M. N. Klein, " σ -Noninnocence: Masked Phenyl-Cation Transfer at Formal Ni^{IV}," *Angew. Chem., Int. Ed.* **58**, 13133–13139 (2019).
- ¹³⁶B. Senjean, S. Sen, M. Repisky, G. Knizia, and L. Visscher, "Generalization of Intrinsic Orbitals to Kramers-Paired Quaternion Spinors, Molecular Fragments, and Valence Virtual Spinors," *J. Chem. Theory Comput.* **17**, 1337–1354 (2021).
- ¹³⁷As there are n_{\min} IAOs and we project out n_{occ} IBOs whose span is very close (but not identical) to a subset of the span of the IAOs, we expect to get $n_{\min} - n_{\text{occ}}$ linearly independent orbitals from the singular value decomposition.
- ¹³⁸P. A. Kalozoumis, C. Morfonios, F. K. Diakonou, and P. Schmelcher, "Local symmetries in one-dimensional quantum scattering," *Phys. Rev. A* **87**, 032113 (2013).
- ¹³⁹P. Schmelcher, S. Krönke, and F. K. Diakonou, "Dynamics of local symmetry correlators for interacting many-particle systems," *J. Chem. Phys.* **146**, 044116 (2017).
- ¹⁴⁰A. I. Kuleff, "Electronic decay through carbon chains," *Chem. Phys.* **482**, 216–220 (2017).
- ¹⁴¹F. Mauger, A. S. Folorunso, K. A. Hamer, C. Chandre, M. B. Gaarde, K. Lopata, and K. J. Schafer, "Charge migration and attosecond solitons in conjugated organic molecules," *Phys. Rev. Res.* **4**, 013073 (2022).
- ¹⁴²This assumes that the first excited state is approximately described by an orbital excitation.
- ¹⁴³For simplicity, we avoid here the introduction of additional arrows that would depict the motion of a hole/positive charge.
- ¹⁴⁴This mechanism is independent from a negative hole density appearing in the phenyl ring, which appears for all three dynamics and is due to 2h1p configurations and global symmetry changes discussed later.
- ¹⁴⁵Note that quantifying these interactions is beyond the scope of this work.
- ¹⁴⁶The unprojected hole densities are semi-quantitatively identical to the projected ones and are shown in Supplementary Fig. S7.
- ¹⁴⁷"block2," (2024), <https://github.com/block-hczhai/block2-preview>.
- ¹⁴⁸Q. Sun, T. C. Berkelbach, N. S. Blunt, G. H. Booth, S. Guo, Z. Li, J. Liu, J. D. McClain, E. R. Sayfutyarova, S. Sharma, S. Wouters, and G. K.-L. Chan, "PySCF: the Python-based simulations of chemistry framework," *Wiley Interdiscip. Rev.: Comput. Mol. Sci.* **8**, e1340 (2018).
- ¹⁴⁹Q. Sun, X. Zhang, S. Banerjee, P. Bao, M. Barbry, N. S. Blunt, N. A. Bogdanov, G. H. Booth, J. Chen, Z.-H. Cui, J. J. Eriksen, Y. Gao, S. Guo, J. Hermann, M. R. Hermes, K. Koh, P. Koval, S. Lehtola, Z. Li, J. Liu, N. Mardirossian, J. D. McClain, M. Motta, B. Mussard, H. Q. Pham, A. Pulkin, W. Purwanto, P. J. Robinson, E. Ronca, E. R. Sayfutyarova, M. Scheurer, H. F. Schurkus, J. E. T. Smith, C. Sun, S.-N. Sun, S. Upadhyay, L. K. Wagner, X. Wang, A. White, J. D. Whitfield, M. J. Williamson, S. Wouters, J. Yang, J. M. Yu, T. Zhu, T. C. Berkelbach, S. Sharma, A. Y. Sokolov, and G. K.-L. Chan, "Recent developments in the PySCF program package," *J. Chem. Phys.* **153**, 024109 (2020).
- ¹⁵⁰"PySCF," (2024), <https://github.com/pyscf/pyscf>.
- ¹⁵¹W. Tatsuaki, "Interaction-round-a-face density-matrix renormalization-group method applied to rotational-invariant quantum spin chains," *Phys. Rev. E* **61**, 3199–3206 (2000).
- ¹⁵²S. Sharma and G. K.-L. Chan, "Spin-adapted density matrix renormalization group algorithms for quantum chemistry," *J. Chem. Phys.* **136**, 124121 (2012).
- ¹⁵³T. J. Park and J. C. Light, "Unitary quantum time evolution by iterative Lanczos reduction," *J. Chem. Phys.* **85**, 5870–5876 (1986).
- ¹⁵⁴R. Ditchfield, W. J. Hehre, and J. A. Pople, "Self-Consistent Molecular-Orbital Methods. IX. An Extended Gaussian-Type Basis for Molecular-Orbital Studies of Organic Molecules," *J. Chem. Phys.* **54**, 724–728 (1971).
- ¹⁵⁵W. J. Hehre, R. Ditchfield, and J. A. Pople, "Self-Consistent Molecular Orbital Methods. XII. Further Extensions of Gaussian-Type Basis Sets for Use in Molecular Orbital Studies of Organic Molecules," *J. Chem. Phys.* **56**, 2257–2261 (1972).
- ¹⁵⁶F. Weigend and R. Ahlrichs, "Balanced basis sets of split valence, triple zeta valence and quadruple zeta valence quality for H to Rn: Design and assessment of accuracy," *Phys. Chem. Chem. Phys.* **7**, 3297–3305 (2005).
- ¹⁵⁷A. I. Kuleff, N. V. Kryzhevoi, M. Pernpointner, and L. S. Cederbaum, "Core ionization initiates subfemtosecond charge migration in the valence shell of molecules," *Phys. Rev. Lett.* **117**, 093002 (2016).